Kinetic Mechanisms of the Nucleotide Cofactor Binding to the Strong and Weak Nucleotide-Binding Site of the *Escherichia coli* PriA Helicase. 2†

Aaron L. Lucius, Maria J. Jezewska, Anasuya Roychowdhury, and Wlodzimierz Bujalowski*

Department of Biochemistry and Molecular Biology, Department of Obstetrics and Gynecology, The Sealy Center for Structural Biology, Sealy Center for Cancer Cell Biology, The University of Texas Medical Branch at Galveston, 301 University Boulevard, Galveston, Texas 77555-1053

Received September 9, 2005; Revised Manuscript Received March 8, 2006

ABSTRACT: Kinetics of the nucleotide binding to the strong (S) and weak (W) nucleotide-binding site of the *Escherichia coli* PriA helicase have been studied using the fluorescence stopped-flow technique. Experiments were performed with TNP-ADP and TNP-ATP analogues. Binding of the ADP analogue to the strong binding site is a four-step sequential reaction: $(PriA)_S + D \overset{k_1}{\underset{k_{-1}}{\rightleftarrows}} + (S)_1 \overset{k_2}{\underset{k_{-2}}{\rightleftarrows}} (S)_2 \overset{k_3}{\underset{k_{-3}}{\rightleftarrows}} (S)_3 \overset{k_4}{\underset{k_{-4}}{\rightleftarrows}} (S)_4$. Association of TNP-ATP proceeds through an analogous three-step mechanism. The first two steps and intermediates are similar for both cofactors. However, the $(S)_3$ intermediate is dramatically different for ADP and ATP analogues. Its emission is close to the emission of the free TNP-ADP, while it is by a factor of ∼16 larger than the free TNP-ATP fluorescence. Thus, only the ADP analogue passes through an intermediate where it leaves the hydrophobic cleft of the site. This behavior corroborates with the fact that ADP leaves the ATPase site without undergoing a chemical change. The fast bimolecular step and the sequential mechanism indicate that the site is easily accessible to the cofactor, and it does not undergo an adjustment prior to binding. The subsequent step is also fast and stabilizes the complex. Magnesium profoundly affects the population of intermediates. The data indicate that the dominant $(S)_2$ species is a part of the ATP catalytic cycle. ADP analogue binding to the weak nucleotide-binding site proceeds in a simpler two-step mechanism: $(PriA)_W + D \overset{k_1}{\underset{k_{-1}}{\rightleftarrows}} (W)_1 \overset{k_2}{\underset{k_{-2}}{\rightleftarrows}} (W)_2$ with $(W)_1$ being a dominant intermediate both in the presence and in the absence of Mg^{2+}. The results indicate that the weak site is an allosteric control site in the functioning of the PriA helicase.

The PriA helicase is a key DNA replication enzyme in *Escherichia coli* cell that plays a fundamental role in the ordered assembly of the primosome, a multiple-protein−DNA complex formed in the process of priming a DNA strand (*1*−*8*). Originally, the PriA helicase was discovered as an essential factor during the synthesis of the complementary DNA strand of phage ΦX174 DNA (*9*−*11*). Current data indicate that the enzyme is involved not only in DNA replication but also in recombination and repair processes in the *E. coli* cell (*12*−*14*).

The unwinding of the duplex nucleic acid by a helicase requires binding and hydrolysis of nucleotide triphosphates (NTPs)[1] (*15*−*20*). In a companion paper (*67*), we have described quantitative equilibrium studies of the PriA helicase−nucleotide cofactor interactions. The obtained data establish that the PriA helicase has two nucleotide-binding sites that differ dramatically in their affinities and properties. The intrinsic affinity of the strong binding site is higher by 2−4 orders of magnitude than the affinity of the weak site. The strong nucleotide-binding site is also highly specific for adenosine cofactors, while the weak site shows only a modest base specificity. Moreover, the affinity of the strong site, unlike the affinity of the weak site, profoundly depends on the structure of the phosphate group of the ATP cofactor. Binding of Mg^{2+} to the cofactor and the protein is specifically involved in controlling the affinity of the nucleotides for the strong site. These properties and available biochemical data indicate that the strong nucleotide-binding site is the dominant ATPase site of the PriA helicase (*21*, *22*). Furthermore, competition studies with unmodified nucleotides indicate the presence of cooperative interactions between the bound cofactors, providing evidence of the communication between the two nucleotide-binding sites (*67*).

Elucidation of the mechanism of binding and the nature of the different complexes between the helicase and nucleotide cofactors is a prerequisite for understanding the mechanism of the free energy transduction during the enzyme functioning in DNA replication and recombination (*21*, *23*−*30*). In the case of the PriA helicase, this is particularly important in the context of the discovery of two nucleotide-binding sites of the enzyme that differ so dramatically in their affinities and properties (*67*). Despite the recognized

† This work was supported by NIH Grant GM-46679 (to W.B.). A.L.L. was partially supported by a J. B. Kempner postdoctoral fellowship.

* Corresponding author. Tel.: (409)772-5634. Fax: (409)772-1790. E-mail.: wbujalow@utmb.edu.

[1] Abbreviations: TNP-ATP, 2′(3′)-*O*-(2,4,6-trinitrophenyl)adenosine triphosphate; TNP-ADP, 2′(3′)-*O*-(2,4,6-trinitrophenyl)adenosine 5′-diphosphate; NTP, nucleoside triphosphate; PAS, primosome assembly site; Tris, tris(hydroxymethyl)aminomethane; DTT, dithiothreitol; EDTA, ethylenediaminetetraacetic acid disodium salt.

10.1021/bi051827e CCC: $33.50
Published on Web 05/20/2006

importance of the PriA helicase−nucleotide interactions, kinetic mechanisms of these interactions have never been addressed.

In this paper, we report the quantitative analyses of the kinetics of the nucleotide cofactor binding to the strong and weak nucleotide-binding sites of the PriA helicase using the fluorescence stopped-flow technique. Binding of the ADP analogue to the strong nucleotide-binding sites of the PriA helicase is a minimum four-step sequential reaction, while the association of the ATP analogue with the same site proceeds through a three-step sequential mechanism. The data indicate that unlike ATP, the ADP analogue passes through an intermediate where it leaves the hydrophobic cleft of the site. Mg^{2+} cations have a profound effect on the populations and the structure of the intermediates. Contrary to the strong site, association of the ADP analogue with the weak site proceeds in a much simpler two-step sequential mechanism, suggesting that the weak site is an allosteric control site of the enzyme (*68*).

MATERIALS AND METHODS

Reagents and Buffers. All chemicals were reagent grade. All solutions were made as described in ref *67*. TNP-ATP and TNP-ADP were from Molecular Probes (Eugene, OR) (*32*). ATP was from CalBiochem. ADP, GDP, CDP, and TDP were from Sigma (St. Louis, MO). The *E. coli* PriA protein has been isolated and purified as described previously (*29*−*31*, *67*).

Fluorescence Measurements. All steady-state fluorescence titrations were performed using the Fluorolog F-11 (Spex Jobin Yvon) as described previously and in a companion paper (*33*−*39*, *67*). Binding of a cofactor to the helicase was followed by monitoring the fluorescence of TNP-ADP or TNP-ATP (λ_{ex} = 408 nm, λ_{em} = 550 nm). Computer fits were performed using Mathematica (Wolfram, IL) and KaleidaGraph (Synergy Software, PA). The relative increase of intensity, ΔF_{obs}, of the cofactor emission upon binding to the PriA helicase is defined as $\Delta F_{obs} = (F_i - F_o)/F_o$, where F_i is the fluorescence of the TNP analogue at a given titration point, and F_o is the initial value of the fluorescence of the sample (*33*−*39*).

Stopped-Flow Kinetics. All fluorescence stopped-flow kinetics experiments were performed using the SX.18MV stopped-flow instrument (Applied Photophysics, Leatherhead, UK) as described before using the linear two time-bases mode (*40*−*46*). The reactions were monitored following the total fluorescence emission of the TNP analogues, with λ_{ex} = 408 nm, and the emission was monitored through the GG500 cutoff filter (Schott, PA). The excitation monochromator slits were at 1.5 mm (band-pass ≈ 7 nm). Eight to fifteen traces were collected and averaged for each sample. The relaxation times and amplitudes for each kinetic trace were determined using the nonlinear, least-squares software, with the exponential function defined as (*47*):

$$F(t) = F(\infty) + \sum_{i=1}^{n} A_i \exp(-\lambda_i t) \qquad (1)$$

where $F(t)$ is the fluorescence intensity at time t, $F(\infty)$ is the fluorescence intensity at time $t = \infty$, A_i is the amplitude corresponding to the ith relaxation process, λ_i is the time constant (reciprocal relaxation time) characterizing the ith relaxation process, and n is the number of relaxation processes. All further analyses of the data were performed using Mathematica (Wolfram, Urbana, IL) and KaleidaGraph (Synergy Software, PA). Kinetic analyses of the stopped-flow data have been performed using the matrix projection operator technique that has been extensively described by us before (*40*−*46*).

RESULTS

Binding of the TNP-ADP Analogue to the PriA Helicase Followed by Monitoring the Fluorescence Intensity of the Nucleotide Cofactor in the Presence of Magnesium. In the studies of the binding of nucleotide analogues, TNP-ADP and TNP-ATP (described in ref *67*), we used the quenching of the protein fluorescence to monitor the interactions. Thus, the binding process was monitored by the changes of the spectroscopic signal, originating from the macromolecule and induced by the nucleotide cofactor binding (*48*, *49*). This is the most intuitive approach, also referred to as a "normal" titration, because the total average degree of binding, $\Sigma\Theta_i$, and the degree of saturation of the protein with the nucleotide are increasing functions of the cofactor concentration in solution. However, although the observed quenching of the PriA fluorescence is adequate to study the thermodynamics of the analogue interactions with the helicase, it is less suitable for examination of the kinetics of the complex formation, particularly at the strong nucleotide-binding site where the binding of the cofactor induces only a moderate relative fluorescence quenching, $\Delta F_1 = 0.20 \pm 0.03$ (*67*). On the other hand, binding of the TNP analogues to the PriA helicase results in a very large increase of the cofactor fluorescence (see below). Such a large signal change, originating from the ligand, allows us to examine the kinetics of the cofactor binding to the strong and weak nucleotide-binding sites of the PriA helicase with required high resolution. Moreover, the fluorescence of the TNP moiety of the nucleotide analogues is very sensitive to the polarity of the environment of the binding site (*35*, *36*, *50*, *51*). Therefore, determination of the relative changes of the analogue emissions accompanying the binding to each binding site of the enzyme provides unique insight into the nature of the binding site and structure of the formed transient intermediates (*40*−*42*, *50*, *51*) (see below).

Fluorescence titrations of TNP-ADP with PriA helicase in buffer C (pH 7.0, 20 °C) containing 20 mM NaCl and 5 mM $MgCl_2$ at three different concentrations of the cofactor are shown in Figure 1. This type of titration, where the ligand is titrated with the macromolecule, is referred to as a "reverse" titration (*48*). The selected [TNP-ADP] concentrations are 1×10^{-6} M, 5×10^{-6} M, and 7×10^{-5} M, respectively. The titration at the highest applied concentration of the cofactor (7×10^{-5} M) could only be performed in limited protein concentration range due to the precipitation of the complex at high protein and nucleotide concentrations (*67*). As the cofactor concentration increases, a given relative fluorescence increase, ΔF_{obs}, is reached at higher protein concentrations because more protein is required to saturate the increased concentration of the nucleotide (*33*, *39*, *48*,

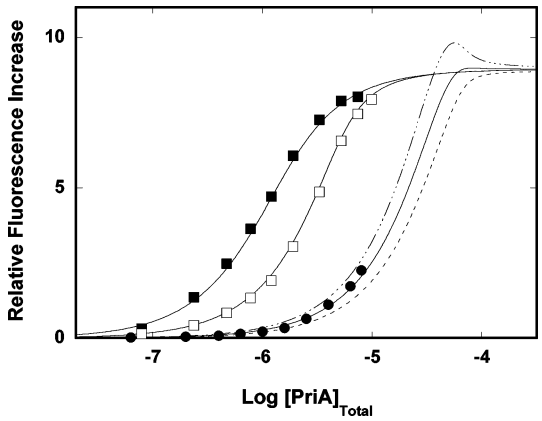

FIGURE 1: (a) Fluorescence titration of TNP-ADP with the PriA helicase in buffer C (pH 7.0, 20 °C) containing 20 mM NaCl and 5 mM $MgCl_2$ at three different TNP-ADP concentrations: (■) 1.0×10^{-6} M; (□) 5.0×10^{-6} M; (●) 7.0×10^{-5} M. The solid lines are nonlinear least-squares fits of the titration curves using eqs 2−6, with a single set of binding parameters $K_{B_1} = 1.5 \times 10^6$ M^{-1}, $K_{B_2} = 1.9 \times 10^4$ M^{-1}, $\sigma = 1$, $\Delta F_{1_{max}} = 9.0$, and $\Delta F_{2_{max}} = 4.3$. The lines (---) and (−---−) are computer simulations of the observed relative fluorescence increase, ΔF_{obs}, as a function of the logarithm of the total PriA concentrations (eq 6) for the sample containing 7.0×10^{-5} M TNP-ADP, using the same binding parameters as above, but different values of the relative fluorescence increase accompanying the binding to the weak nucleotide -binding site; $\Delta F_{2_{max}} = 0$ (---), $\Delta F_{2_{max}} = 9.0$ (−---−).

49). The same value of the relative fluorescence increase at the plateaus for the two lower total TNP-ADP concentrations, at saturation, results from the fact that, although the titrations start at different degrees of binding, they end up at the same complete cofactor saturation by the protein.

In the absence of any knowledge about the examined interacting system, quantitative analysis of the data in Figure 1 would require the ligand binding density function approach to construct the thermodynamic binding isotherm (*39*, *48*). On the other hand, in the considered case of TNP-ADP binding to the PriA protein, we know the statistical thermodynamic model that describes the observed binding process and the values of all binding parameters in the model (*67*). Notice, although the physical nature of the observed spectroscopic signal is different, the binding process and the intrinsic binding parameters must be the same. Thus, there are two discrete nucleotide-binding sites on the enzyme characterized by the intrinsic binding constants, K_{B_1} and K_{B_2}, and the cooperativity parameter, $\sigma = 1$, for TNP-ADP (*67*). The binding process is complex and the binding isotherm cannot be analytically described by a single equation. The total partition function, Z, and the total average degree of binding, $\Sigma\Theta_i$, of the considered system are described as in a companion paper (*67*), by (*52*)

$$Z = 1 + (K_{B_1} + K_{B_2})L_F + K_{B_1}K_{B_2}\sigma L_F^2 \qquad (2a)$$

$$\Sigma\Theta_i = \frac{(K_{B_1} + K_{B_2})L_F + 2K_{B_1}K_{B_2}\sigma L_F^2}{Z} \qquad (2b)$$

The total nucleotide cofactor concentration, L_T, is related to its free concentration by a mass conservation equation

$$L_T = L_F[1 + (K_{B_1} + K_{B_2})P_F] + 2K_{B_1}K_{B_2}\sigma L_F^2 P_F \quad (3)$$

where P_F is the free concentration of the PriA protein. This is a second-degree polynomial that can be analytically solved for L_F with the physically acceptable solution as

$$L_F = \frac{-(1 + K_{B_1} + K_{B_2})P_F + \sqrt{[1 + (K_{B_1} + K_{B_2})P_F]^2 + 8K_{B_1}K_{B_2}\sigma L_T P_F}}{4K_{B_1}K_{B_2}\sigma P_F} \qquad (4)$$

Thus, the concentration of the free cofactor can be obtained as a unique function of the known binding parameters and the known total concentrations of the nucleotide cofactor, L_T, and the free protein concentration, P_F. Expression 4 is the first required parametric equation.

The second parametric equation is the expression for the total protein concentration, P_T, as a function of the free protein concentration, P_F, that is:

$$P_T = P_F[1 + (K_{B_1} + K_{B_2})L_F + K_{B_1}K_{B_2}\sigma L_F^2] \qquad (5)$$

Thus, the free nucleotide concentration, L_F, and the total protein concentration, P_T, are described as unique functions of the free protein concentration, P_F, which is the independent variable. The observed relative fluorescence increase, ΔF_{obs}, of the nucleotide analogue in the presence of the helicase is then described by

$$\Delta F_{obs} = \Delta F_{1_{max}}\left(\frac{K_{B_1}L_F P_F}{L_T}\right) + \Delta F_{2_{max}}\left(\frac{K_{B_2}L_F P_F}{L_T}\right) + (\Delta F_{1_{max}} + \Delta F_{2_{max}})\left(\frac{K_{B_1}K_{B_2}\sigma L_F^2 P_F}{L_T}\right) \qquad (6)$$

where L_T is defined by eq 3. The parameters $\Delta F_{1_{max}}$ and $\Delta F_{2_{max}}$ are the maximum relative fluorescence increase of the nucleotide cofactor emission bound to the strong and weak nucleotide-binding sites, respectively. Computer simulation and/or fitting are performed by first calculating the free cofactor concentration, L_F, for a given set of the binding parameters K_{B_1}, K_{B_2}, and σ and the selected value of P_F using eq 4. The total average degree of binding, $\Sigma\Theta_i$, and corresponding total protein concentration, P_T, are calculated for the same values of P_F and obtained L_F, using eqs 2b and 5. Subsequently, both P_F and L_F are introduced to eq 6 to obtain ΔF_{obs}.

Binding of TNP-ADP to the strong and weak nucleotide binding site of the PriA helicase is characterized by $K_{B_1} = (1.5 \pm 0.5) \times 10^6$ M^{-1}, $K_{B_2} = (1.9 \pm 0.6) \times 10^4$ M^{-1}, and $\sigma = 1 \pm 0.3$, determined independently using protein fluorescence quenching to monitor the binding (*67*). For such a large difference in affinities between the binding sites, eq 6 indicates that, at saturating protein concentrations, only the first term contributes to the observed fluorescence (i.e., all titration curves tend to the maximum fluorescence increase, $\Delta F_{1_{max}}$). Analogously, at [TNP-ADP] concentrations $\leq 5 \times 10^{-6}$ M, predominantly, the binding to the strong site will occur. In such a situation, eq 6 reduces to

$$\Delta F_{obs} = \Delta F_{1_{max}}\left(\frac{K_{B_1}L_F P_F}{L_T}\right) \qquad (7)$$

Thus, the relative fluorescence increases of the titration curves obtained for the two low concentrations of TNP-ADP tend to the plateau $\approx \Delta F_{1_{max}}$.

The situation is different for the titrations of TNP-ADP with the PriA helicase performed at [TNP-ADP] $= 7 \times 10^{-5}$ M, shown in Figure 1. At this concentration of the cofactor, the weak nucleotide-binding site, characterized by $K_{B_2} \approx 1.9 \times 10^4$ M^{-1}, becomes significantly saturated with the nucleotide (*67*). The solid lines in Figure 1 are nonlinear least-squares fits of the experimental titration curves, using eq 6, with $K_{B_1} = 1.5 \times 10^6$ M^{-1}, $K_{B_2} = 1.9 \times 10^4$ M^{-1}, and $\sigma = 1$ (*67*), and only two fitting parameters, $\Delta F_{1_{max}}$ and $\Delta F_{2_{max}}$, which provide $\Delta F_{1_{max}} = 9.0 \pm 0.3$ and $\Delta F_{2_{max}} = 4.3 \pm 1$, respectively. The single set of the spectroscopic and binding parameters gives an excellent representation of the binding system over the entire studied range of the nucleotide concentration. For comparison, the theoretical titration curves with different values of $\Delta F_{2_{max}}$ for the titration performed at the highest examined cofactor concentration are also included in Figure 1. Notice, the values of ΔF_{obs} may exceed the value of $\Delta F_{1_{max}}$ at intermediate protein concentrations, although return to the plateau at saturation (Figure 1). This results from the contribution of the PriA−cofactor complex containing two nucleotide molecules at intermediate protein concentrations (third term in eq 6). It is evident that, in the presence of magnesium, the binding of TNP-ADP to the weak nucleotide-binding site is accompanied by substantial, ~4-fold increase of the cofactor fluorescence. Nevertheless, this value is still significantly lower than the relative increase of the cofactor fluorescence, $\Delta F_{1_{max}} = 9.0 \pm 0.3$, accompanying the binding to the strong nucleotide-binding site (see the Discussion).

Kinetics of the TNP-ADP Binding to the Strong Nucleotide-Binding Site of the PriA Helicase in the Presence of Magnesium. The 2 orders of magnitude difference between the affinities of the two nucleotide-binding sites of the enzyme that allows us to examine the nucleotide binding to each site, independent from each other (Figure 1), allows us also to examine the kinetics of the binding process at a given site, independent of the cofactor binding to the other site (see below). In the first set of experiments, we addressed the dynamics of the ADP analogue, TNP-ADP, binding exclusively to the strong nucleotide-binding site of the PriA helicase.

The fluorescence stopped-flow kinetic trace after mixing 1×10^{-6} M TNP-ADP with 1.8×10^{-5} M PriA (final concentrations) in buffer C (pH 7.0, 20 °C) containing 20 mM NaCl and 5 mM $MgCl_2$ is shown in Figure 2a. To increase the resolution, the plot is shown in logarithmic scale with respect to time. The initial horizontal part of the trace corresponds to the steady-state fluorescence intensity of the sample, recorded for ~2 ms in our instrument, before the flow stops (*44*−*46*). The solid line in Figure 2a is a nonlinear least-squares fit of the experimental trace, using a three-exponential fit, as defined by eq 1. The included two-exponential function does not provide an adequate description of the observed kinetics (dashed line). Using a larger number of exponents in the fitting function (eq 1) does not improve the statistics of the fit (data not shown).

The stopped-flow kinetic trace, together with the trace corresponding to the TNP-ADP alone, at the same concentration of the cofactor as used with the protein but only mixed with the buffer (zero line) is shown in Figure 2b. The total amplitude of the trace is the difference between the zero line and the fluorescence intensity at time, $t = \infty$ (*40*−*46*, *53*, *54*). As we discussed before, comparison between the resolved relaxation amplitudes and the total amplitude of the kinetic trace is crucial in establishing that the resolved relaxation processes account for the total observed signal (*40*−*46*). The three-exponential fit provides an excellent description of the observed kinetic process. However, it clearly does not account for the total amplitude of the overall relaxation process. These data indicate that an additional fast process, which is beyond the time-resolution of the stopped flow technique, precedes the observed relaxation processes. Thus, the binding of TNP-ADP to the strong nucleotide-binding site of the PriA helicase occurs in at least four steps. The reciprocal relaxation times ($1/\tau_2$, $1/\tau_3$, and $1/\tau_4$) extracted from the experimental trace as a function of the total PriA concentration are shown in panels a−c of Figure 3. The value

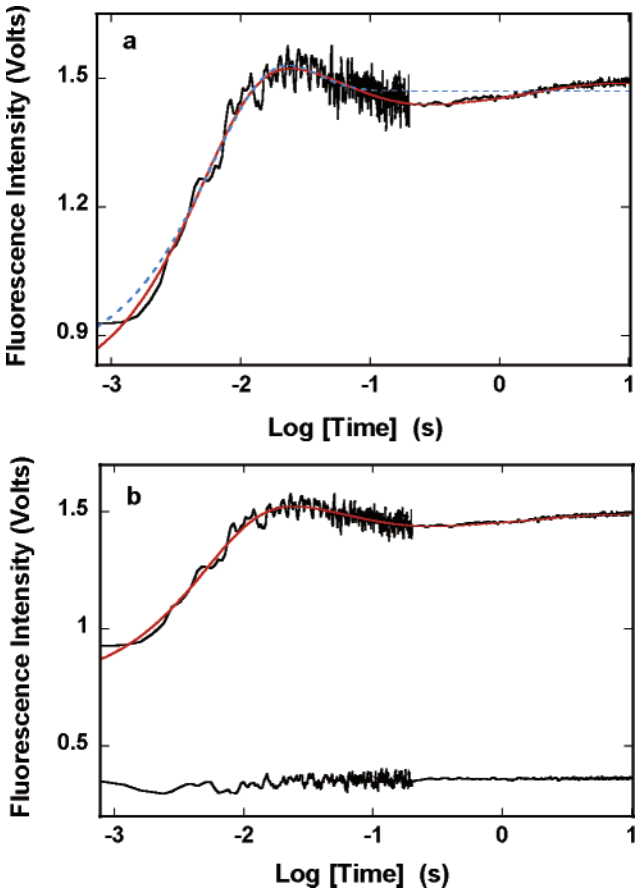

FIGURE 2: (a) Fluorescence stopped-flow kinetic trace, after mixing TNP-ADP with the PriA helicase in buffer C (pH 7.0,20 °C) containing 20 mM NaCl and 5 mM $MgCl_2$ ($\lambda_{ex} = 408$ nm, $\lambda_{em} > 500$ nm). The final concentrations of the cofactor and the helicase are 1×10^{-6} M and 1.8×10^{-5} M, respectively. The experimental kinetic trace is shown in logarithmic scale with respect to time. The initial horizontal part of the trace is the steady-state value of the fluorescence of the sample recorded for ~2 ms before the flow stopped (Materials and Methods). The solid red line is the three-exponential, nonlinear least-squares fit of the experimental curve using eq 1. The dashed blue line is the nonlinear least-squares fit using the two-exponential function (eq 1). (b) The same fluorescence stopped-flow trace as in panel a together with the zero line trace (lower green trace), which is obtained after mixing TNP-ADP only with the buffer. The solid red line is the same three-exponential, nonlinear least-squares fit of the experimental curve as shown in Figure 3a.

Scheme 1

$$(\mathbf{PriA})_S + \mathbf{D} \underset{k_{-1}}{\overset{k_1}{\leftrightarrow}} (S)_1 \underset{k_{-2}}{\overset{k_2}{\leftrightarrow}} (S)_2 \underset{k_{-3}}{\overset{k_3}{\leftrightarrow}} (S)_3 \underset{k_{-4}}{\overset{k_4}{\leftrightarrow}} (S)_4$$

of $1/\tau_2$ shows a slight dependence upon [PriA] while both $1/\tau_3$ and $1/\tau_4$ are, within experimental accuracy, independent of the helicase concentration. Such behavior indicates that all three relaxation times characterize the intramolecular transitions of the formed complex (*40*−*46*, *53*, *54*). Therefore, the simplest minimum mechanism, which can account for the observed dependence of the relaxation times upon the PriA concentration and the presence of the unresolved process is a four-step, sequential binding reaction in which a bimolecular association is followed by three isomerization of the formed complex, as described by Scheme 1.

Although the relaxation time, τ_1, for the fast normal mode of the reaction cannot be determined, the amplitude of this mode, A_1, can be obtained from the known amplitudes of the second, third, and fourth normal modes (A_2, A_3, and A_4) and the total amplitude (A_T) as

$$A_1 = A_T - A_2 - A_3 - A_4 \tag{8}$$

The dependence of the individual amplitudes A_1, A_2, A_3, and A_4 of the four relaxation modes upon the PriA concentration is shown in Figure 3d. The individual amplitudes are expressed as fractions of the total amplitude, $A_i/\Sigma A_i$. In the examined [enzyme] range, all four amplitudes contribute to A_T, even at the lowest [enzyme]. The amplitude A_2 is always positive and dominates the observed relaxation process over the entire examined range of the applied protein concentration. The amplitude A_3 is negative and is independent of the PriA concentration. Amplitude A_4 is positive and has very small values. On the other hand, initially, A_1 has a small positive value and as the concentration of the helicase increases, the values of A_1 increase and become comparable to the values of the dominant amplitude A_2.

Because only three relaxation times are available from the experiment, determination of rate constants of particular steps and molar fluorescence parameters characterizing each intermediate requires the simultaneous analyses of both the relaxation times and the amplitudes. We applied the following strategy to obtain the rate and spectroscopic parameters of the system (*40*−*46*). We utilized the fact that we know the value of the intrinsic binding constant $K_{B_1} = (1.5 \pm 0.5) \times 10^6$ M^{-1} for the TNP-ADP binding to the strong nucleotide-binding site, independently obtained in the same solution conditions by the equilibrium fluorescence titration method (*67*). The intrinsic binding constant K_{B_1} is related to the partial equilibrium constants characterizing partial equilibrium steps in the binding to the strong site by

$$K_{B_1} = K_1 (1 + K_2 + K_2K_3 + K_2K_3K_4) \tag{9}$$

where $K_1 = k_1/k_{-1}$, $K_2 = k_2/k_{-2}$, $K_3 = k_3/k_{-3}$, and $K_4 = k_4/k_{-4}$. Expression 9 reduces by one the number of the independent parameters in numerical fitting of the three individual relaxation times. Because the unresolved step is very fast, the fits are performed with this step characterized by the partial equilibrium constant, K_1.

The obtained equilibrium and rate constants were then used in the fitting of the four individual amplitudes that include the relative molar fluorescence intensities using the matrix projection operator technique, which allows us to determine the molar fluorescence intensities characterizing each intermediate of the reaction (i.e., to assess the conformational state of the cofactor−PriA complex in each intermediate in the strong nucleotide-binding site). Here, we utilize the fact that the maximum, fractional increase of the cofactor fluorescence, $\Delta F_{1_{max}} = 9.0 \pm 0.3$, is known from the equilibrium titrations (Figure 1). The value of $\Delta F_{1_{max}}$ can be analytically expressed in terms of the partial steps as (*40*−*46*)

$$\Delta F_{1_{max}} = \frac{\Delta F_1 + K_2\Delta F_2 + K_2K_3\Delta F_3 + K_2K_3K_4\Delta F_4}{Z_{D1}} \tag{10}$$

where $Z_{D1} = 1 + K_2 + K_2K_3 + K_2K_3K_4$, $\Delta F_1 = (F_{S_1} - F_F)/F_F$, $\Delta F_2 = (F_{S_2} - F_F)/F_F$, $\Delta F_3 = (F_{S_3} - F_F)/F_F$, and $\Delta F_4 = (F_{S_4} - F_F)/F_F$ are fractional fluorescence intensities of each intermediate in the binding of TNP-ADP to the strong nucleotide-binding site of the PriA helicase relative to the molar fluorescence intensity of the free cofactor in solution, F_F. Notice, contrary to ΔF_i, the fluorescence parameters F_{S_1}, F_{S_2}, F_{S_3}, and F_{S_4} are relative molar fluorescence intensities with respect to the fluorescence of the free cofactor. Equation 10 provides an additional relationship between the fluorescence parameters, with $\Delta F_{1_{max}}$ playing the role of a scaling factor. In the final step of the analysis, global fitting that simultaneously includes all relaxation times and amplitudes refined the values of the rate constants and spectroscopic parameters. The solid lines in Figure 3 are nonlinear least-squares fits of the relaxation times and amplitudes, according to the mechanism defined by Scheme 1, using a single set of the parameters. The obtained rate constants and relative molar fluorescence parameters are included in Table 1.

The value of $K_1 = (1.0 \pm 0.3) \times 10^5$ M^{-1} indicate that the bimolecular step has a dominant contribution to the free energy, $\Delta G°$, of the cofactor binding. It is a very fast step and must proceed in the time range below ~1 ms. The transition, $(S)_1 \leftrightarrow (S)_2$, with forward rate constant $k_2 = 300 \pm 50$ s^{-1} is also fast and proceeds in a few millisecond time range. The value of the partial equilibrium constants, $K_2 = 15 \pm 8$, indicates that the second step in the mechanism (Scheme 1) contributes significantly and favorably to the overall free energy of binding. However, the final two steps, $(S)_2 \leftrightarrow (S)_3$ and $(S)_3 \leftrightarrow (S)_4$, are dramatically slower than the first two steps with the forward rate constant, k_3 and k_4, being approximately 2 and 3 orders of magnitude lower than k_2 (Table 1). Moreover, these two final steps have negative contributions to the overall free energy of binding with $K_3 = 0.13 \pm 0.07$ and $K_4 = 0.5 \pm 0.2$ (Table 1). Amplitude analysis indicates that the first intermediate, $(S)_1$, is characterized by the relative molar fluorescence intensity 5-fold larger than the emission of the free TNP-ADP ($F_{S_1} = 5.1 \pm 0.3$). The transition to the $(S)_2$ intermediate induces a further, ~100%, increase of the cofactor fluorescence over $(S)_1$ with $F_{S_2} = 11.1 \pm 0.3$. Strikingly, transitions to the $(S)_3$ intermediate is accompanied by a very strong decrease of the bound cofactor fluorescence ($F_{S_3} = 1.3 \pm 0.1$), which becomes comparable to the fluorescence intensity of the free cofactor, while the relative molar fluorescence intensity of the $(S)_4$ intermediate, has the highest value of all intermediates (see the Discussion).

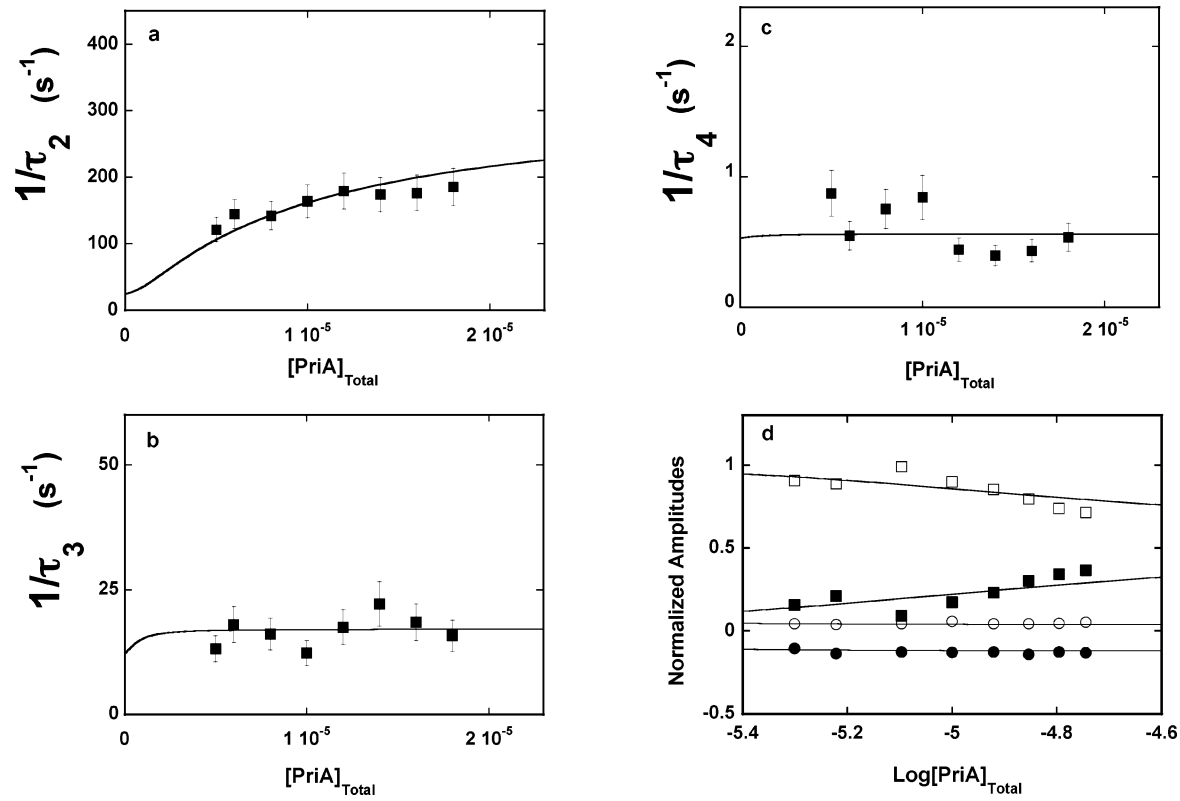

FIGURE 3: Dependence of the reciprocal relaxation times for the TNP-ADP binding to the strong nucleotide-binding site of the PriA helicase in buffer C (pH 7.0, 20 °C) containing 20 mM NaCl and 5 mM $MgCl_2$ upon the total concentration of the enzyme. The solid lines are nonlinear least-squares fits according to the four-step sequential mechanism, defined by Scheme 1, with the equilibrium and rate constants: $K_1 = 1.0 \times 10^5$ M^{-1}, $k_2 = 300$ s^{-1}, $k_{-2} = 20$ s^{-1}, $k_3 = 2$ s^{-1}, $k_{-3} = 15$ s^{-1}, $k_4 = 0.27$ s^{-1}, and $k_{-4} = 0.54$ s^{-1} (details in text). (a) $1/\tau_2$. (b) $1/\tau_3$. (c) $1/\tau_4$. The error bars are standard deviations obtained from 3 to 4 independent experiments. (d) The dependence of the normalized relaxation amplitudes A_1, A_2, A_3, and A_4 for the binding of TNP-ADP to the PriA helicase in buffer C (pH 7.0, 20 °C) containing 20 mM NaCl and 5 mM $MgCl_2$ upon the logarithm of the total enzyme concentration. The solid lines are nonlinear least-squares fits according to the four-step sequential mechanism, defined by Scheme 1, with the relative fluorescence intensities $F_{S_1} = 5.1$, $F_{S_2} = 11.1$, $F_{S_3} = 1.3$, and $F_{S_4} = 16$. The maximum nucleotide fluorescence increase is taken from the equilibrium fluorescence titration in the same solution conditions as $\Delta F_{1_{max}} = 9.1$ (details in text). The rate constants are the same as in panels a−c: (■) A_1, (□) A_2, (●) A_3, and (○) A_4.

Kinetics of the TNP-ATP Binding to the Strong Nucleotide-Binding Site of the PriA Helicase in the Presence of Magnesium. In the case of the ATP analogue TNP-ATP, we could not perform the same equilibrium fluorescence titrations as described for the ADP analogue TNP-ADP (Figure 1) because the PriA helicase hydrolyzes the TNP-ATP on the time scale of the binding experiment, ~60 min (*67*). On the other hand, this behavior indicates that the ATP analogue is in the proper orientation in the binding site to enter the catalytic step (see the Discussion). Nevertheless, we could determine the fractional increase of the TNP-ATP fluorescence, $\Delta F_{1_{max}}$, upon the binding to the strong site by recording its fluorescence within ~10 s after mixing with the saturating concentration of the enzyme where the extent of the analogue hydrolysis is negligibly small (i.e., below ~1% of the total TNP-ATP concentration; data not shown). The obtained value of $\Delta F_{1_{max}} = 8.7 \pm 0.3$. Thus, association with the strong site induces a large increase of the ATP analogue fluorescence, similar to the ADP analogue ($\Delta F_{1_{max}} = 9.0 \pm 0.3$).

The fluorescence stopped-flow kinetic trace after mixing 1×10^{-6} M TNP-ATP with 1.8×10^{-5} M PriA (final concentrations) in buffer C (pH 7.0, 20 °C) containing 20 mM NaCl and 5 mM $MgCl_2$ is shown in Figure 4a. In the examined protein concentration range, the equilibrium state of the association process was reached within ~5 s. Therefore, the stopped-flow traces were recorded over a time period of 5 s to avoid any slow hydrolysis of the cofactor by the enzyme in the presence of magnesium (*67*). Kinetics of the ATP analogue binding to the strong nucleotide-binding site of the PriA helicase is different from the kinetics of the ADP analogue binding. The solid line in Figure 4a is a nonlinear least-squares fit of the experimental trace using a two-exponential function (eq 1). The single-exponential function does not describe the observed relaxation process (dashed line). In addition, using a larger number of exponents in the fitting function (eq 1) does not improve the statistics of the fit (data not shown). The stopped-flow kinetic trace together with the zero line is shown in Figure 4b. It is evident that the two-exponential fit does not account for the total amplitude of the overall relaxation process. Therefore, similar to the ADP analogue, there must be an additional fast process, characterized by a relaxation time, τ_1, which precedes the observed relaxation steps and is too short to be resolved in the stopped-flow experiments (*44*−*46*). The reciprocal relaxation times of the resolved normal modes of the reaction $1/\tau_2$ and $1/\tau_3$ extracted from the stopped-flow traces as a function of the total PriA concentration are shown in panels a and b of Figure 5. The value of $1/\tau_2$ shows a hyperbolic dependence upon [PriA] while the values of $1/\tau_3$ are independent of the helicase concentration, indicating that both relaxation times characterize the intramolecular transitions of the formed complex (see above) (*44*−*46*, *53*, *54*). The simplest mechanism that can account for such behavior of the relaxation times is a three-step, sequential binding

Table 1: Kinetic, Thermodynamic, and Spectroscopic Parameters Characterizing the Binding of TNP-ADP and TNP-ATP to the Strong Nucleotide-Binding Site of the *E. coli* PriA Helicase in Buffer C (pH 7.0, 20 °C) Containing 20 mM NaCl and 5 mM $MgCl_2$ or 0.1 mM EDTA

buffer	k_2 (s^{-1})	k_{-2} (s^{-1})	k_3 (s^{-1})	k_{-3} (s^{-1})	k_4 (s^{-1})	k_{-4} (s^{-1})	K_1 (M^{-1})	K_2	K_3	K_4	overall binding constant (M^{-1})	F_{S_1}	F_{S_2}	F_{S_3}	F_{S_4}
							TNP-ADP								
C 5 mM $MgCl_2$	300 ± 50	20 ± 5	2.0 ± 0.5	15.0 ± 3.5	0.27 ± 0.05	0.54 ± 0.10	(1.0 ± 0.3) × 10^5	15 ± 8	0.13 ± 0.07	0.5 ± 0.2	(1.9 ± 0.6) × 10^6	5.1 ± 0.3	11.1 ± 0.3	1.3 ± 0.1	16.0 ± 0.3
C 0.1 mM EDTA	170 ± 40	40 ± 10	5.1 ± 0.5	1.3 ± 0.3	0.125 ± 0.035	0.025 ± 0.006	(5 ± 1.5) × 10^5	4.3 ± 2.2	3.9 ± 1.4	5.0 ± 1.5	(5.3 ± 1.5) × 10^7	9.4 ± 0.3	20.2 ± 0.4	11.0 ± 0.4	13.1 ± 0.4
							TNP-ATP								
C 5 mM $MgCl_2$	580 ± 100	15 ± 3	1.0 ± 0.2	11.0 ± 2.5			(1.0 ± 0.4) × 10^5	39 ± 15	0.09 ± 0.04		(4.3 ± 1.5)	5.8 ± 0.3	9.2 ± 0.3	15.6 ± 0.1	
C 0.1 mM EDTA	88 ± 20	5.0 ± 1.5	4.0 ± 1.1	0.30 ± 0.06			(5 ± 1.5) × 10^5	17.6 ± 10.2	13.3 ± 6.6		(1.3 ± 0.4) × 10^8	6.3 ± 0.3	16.8 ± 0.3	10.1 ± 0.3	

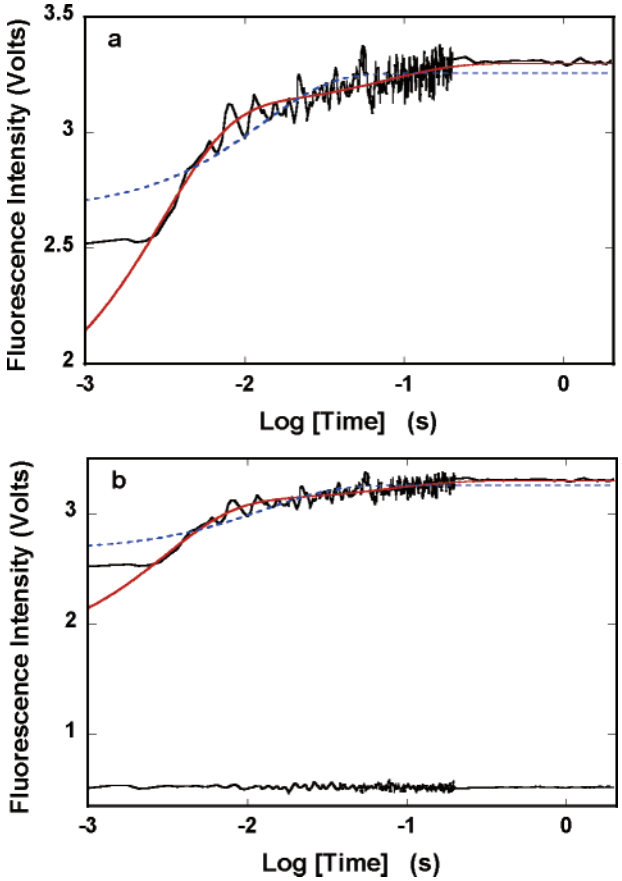

FIGURE 4: (a) Fluorescence stopped-flow kinetic trace, after mixing TNP-ATP with the PriA helicase in buffer C (pH 7.0, 20 °C) containing 20 mM NaCl and 5 mM $MgCl_2$ (λ_{ex} = 408 nm, λ_{em} > 500 nm). The final concentrations of the cofactor and the helicase are 1 × 10^{-6} M and 1.8 × 10^{-5} M, respectively. The experimental kinetic trace is shown in logarithmic scale with respect to time. The initial horizontal part of the trace is the steady-state value of the fluorescence of the sample recorded ~2 ms before the flow stopped (Materials and Methods). The solid red line is the two-exponential, nonlinear least-squares fit of the experimental curve using eq 1. The dashed blue line is the nonlinear least-squares fit using the single-exponential function. (b) The same fluorescence stopped-flow trace as in panel a together with the zero line trace (lower green trace), which is obtained after mixing TNP-ATP only with the buffer. The solid red line is the same three-exponential, nonlinear least-squares fit of the experimental trace as shown in panel a.

reaction in which a bimolecular association is followed by two isomerization steps, as described by Scheme 2. In other words, these data indicate that, unlike the ADP analogue, binding of the nucleotide triphosphate analogue TNP-ATP to the strong nucleotide-binding site of the PriA helicase includes only three sequential steps.

The dependence of the normalized individual amplitudes A_1, A_2, and A_3 of the four relaxation steps upon the PriA concentration is shown in Figure 5c. The amplitude of the fast unresolved mode A_1 has been obtained in an analogous way as described for the TNP-ADP case from the known amplitudes of the second and third normal modes, A_2 and A_3, and the total amplitude of the reaction, A_T, as

$$A_1 = A_T - A_2 - A_3 \tag{11}$$

Unlike the behavior of the ADP analogue (Figures 2a and 3d), all amplitudes of the relaxation modes for the ATP

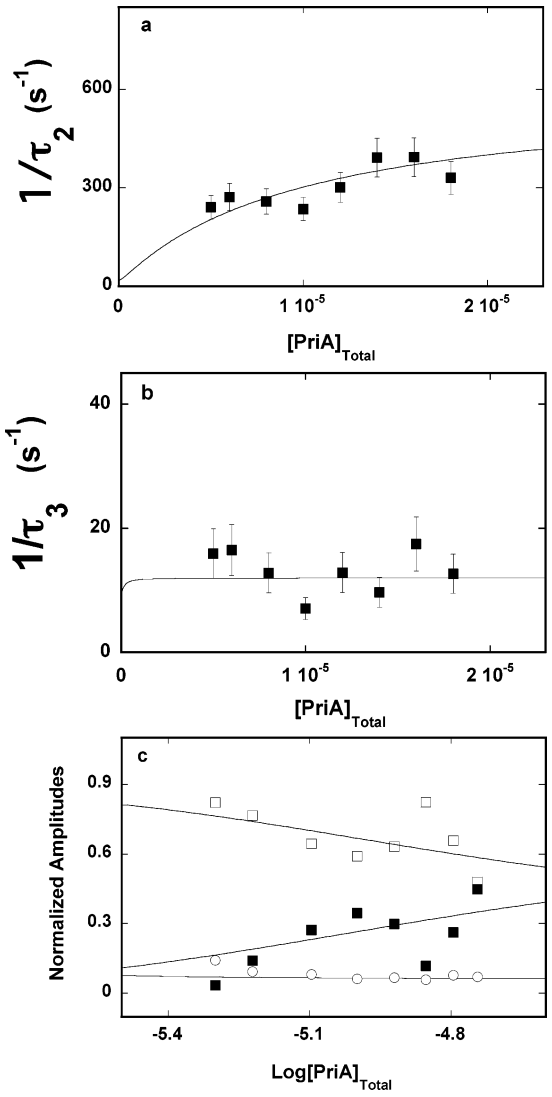

FIGURE 5: Dependence of the reciprocal relaxation times for the binding of TNP-ATP to the strong nucleotide-binding site of the PriA helicase in buffer C (pH 7.0, 20 °C) containing 20 mM NaCl and 5 mM $MgCl_2$ upon the total concentration of the enzyme. The solid lines are nonlinear least-squares fits according to the three-step sequential mechanism, defined by Scheme 2, with the equilibrium and rate constants: $K_1 = 1.0 \times 10^5$ M^{-1}, $k_2 = 580$ s^{-1}, $k_{-2} = 15$ s^{-1}, $k_3 = 1$ s^{-1}, and $k_{-3} = 11$ s^{-1} (details in text). (a) $1/\tau_2$. (b) $1/\tau_3$. The error bars are standard deviations obtained from 3 to 4 independent experiments. (c) The dependence of the normalized relaxation amplitudes [(■) A_1, (□) A_2, and (○) A_3] for the binding of TNP-ATP to the PriA helicase in buffer C (pH 7.0, 20 °C) containing 20 mM NaCl and 5 mM $MgCl_2$ upon the logarithm of the total enzyme concentration. The solid lines are nonlinear least-squares fits according to the three-step sequential mechanism, defined by Scheme 2, with the relative fluorescence intensities $F_{S_1} = 5.8$, $F_{S_2} = 9.2$, and $F_{S_3} = 15.6$ (details in text).

Scheme 2

$$(\mathbf{PriA})_S + \mathbf{T} \underset{\mathbf{k_{-1}}}{\overset{\mathbf{k_1}}{\leftrightarrow}} (\mathbf{S})_1 \underset{\mathbf{k_{-2}}}{\overset{\mathbf{k_2}}{\leftrightarrow}} (\mathbf{S})_2 \underset{\mathbf{k_{-3}}}{\overset{\mathbf{k_3}}{\leftrightarrow}} (\mathbf{S})_3$$

analogue binding to the strong nucleotide-binding site are positive. However, as observed for the ADP analogue, the amplitude A_2 dominates the observed relaxation process over the entire examined range of the protein concentration, although it significantly decreases with the increasing [PriA]. The amplitude A_3 is small and only slightly dependent on the enzyme concentration. The values of the amplitude A_1 of the fast bimolecular step strongly increase as the concentration of the helicase increases, approaching the values of the amplitude A_2 at high [PriA].

Because the value of the overall intrinsic binding constant K_{B_1} for the TNP-ATP binding in the presence of magnesium is not available from the equilibrium data, the determination of the rate constants of individual steps and molar fluorescence parameters, characterizing each intermediate, must exclusively rely on the simultaneous analyses of both the relaxation times and the amplitudes. This does not cause a significant problem in the considered case because the relaxation times of the reaction are strongly separated on the time scale by a factor of at least ~10 (i.e., they are practically "decoupled") (*53*, *54*). The analysis has been initiated by numerical fitting of the two individual relaxation times, with the partial equilibrium constant K_1 and the rate constants k_2, k_{-2}, k_3, and k_{-3} as fitting parameters. The obtained equilibrium and rate constants were then used in the fitting of the three individual amplitudes. Here, we can utilize the fact that the maximum, fractional increase of the ATP analogue fluorescence, $\Delta F_{1_{max}} = 8.7 \pm 0.3$, is known from the independent experiment (see above). In the case of the TNP-ATP, the value of $\Delta F_{1_{max}}$ is analytically defined in terms of the partial steps as (*40*−*46*)

$$\Delta = \frac{\Delta F_1 + K_2 \Delta F_2 + K_2 K_3 \Delta F_3}{Z_{T_1}} \qquad (12)$$

where $Z_{T_1} = 1 + K_2 + K_2K_3$, $\Delta F_1 = (F_{S_1} - F_F)/F_F$, $\Delta F_2 = (F_{S_2} - F_F)/F_F$, and $\Delta F_3 = (F_{S_3} - F_F)/F_F$. In the final step of the analysis, global fitting that simultaneously includes all relaxation times and amplitudes refined the values of the rate constants and spectroscopic parameters. The solid lines in Figure 5 are nonlinear least-squares fits of the relaxation times and amplitudes according to the mechanism defined by Scheme 2, using a single set of the parameters. The obtained rate constants and relative molar fluorescence parameters are included in Table 1.

The obtained data indicate that the bimolecular step has a dominant contribution to the overall free energy of the nucleotide triphosphate binding and its value is the same as obtained for the ADP analogue. However, the following transition $(S)_1 \leftrightarrow (S)_2$ with forward rate constant $k_2 = 580 \pm 50$ s^{-1} is faster than observed for the ADP analogue. On the other hand, the values of the backward rate constant k_{-2} are very similar for both the nucleoside di- and triphosphate. As a result, the partial equilibrium constants, $K_2 = 39 \pm 10$, is larger for the ATP analogue than for the ADP analogue, with the second step (Scheme 2) contributing strongly and favorably to the overall free energy of binding. Contrary to the $(S)_1 \leftrightarrow (S)_2$ transition, the following step $(S)_2 \leftrightarrow (S)_3$ is dramatically slower and contributes negatively to the free energy of binding (Table 1). The data indicate that the overall binding constant, K_{B_1}, for the ATP analogue is slightly larger than the same parameter obtained for the ADP analogue, predominantly, due to the large value of K_2. The relative molar fluorescence intensities characterizing the $(S)_1$ and $(S)_2$ intermediates in the binding of the tri- and diphosphate nucleosides to the strong nucleotide-binding site of the PriA helicase are similar for both cofactors (Table 1). On the other hand, the $(S)_3$ intermediates are dramatically different for the nucleoside di- versus triphosphate, with the molar

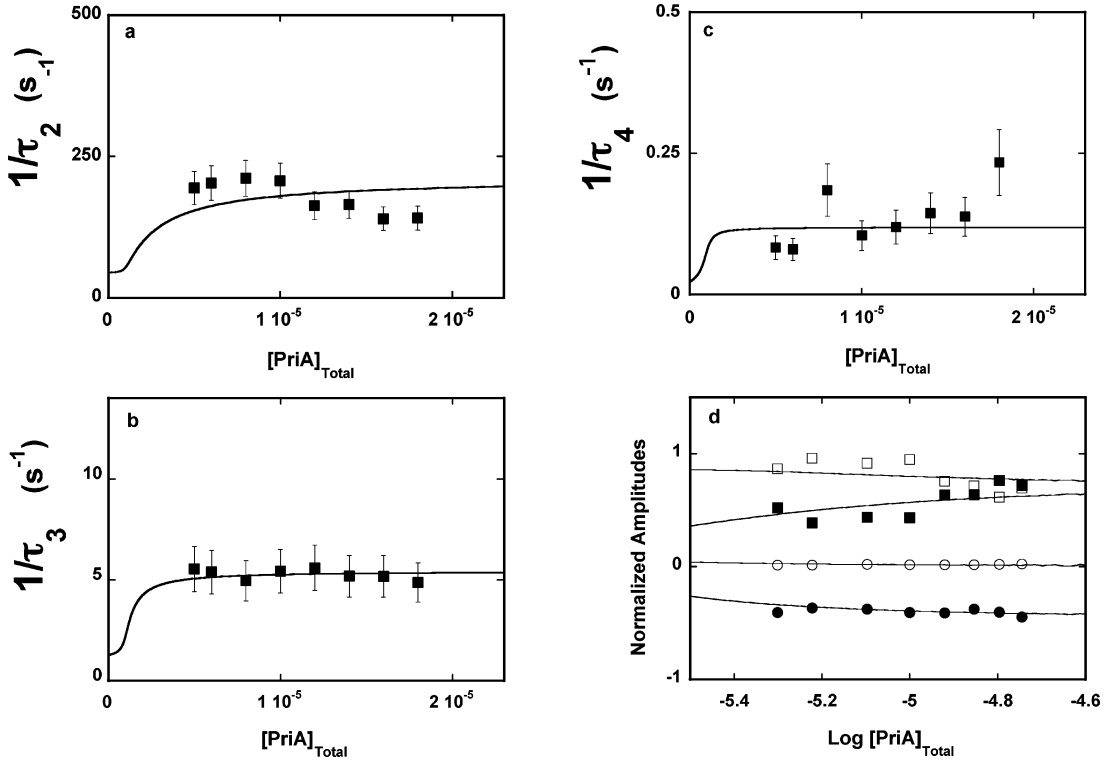

FIGURE 6: Dependence of the reciprocal relaxation times for the TNP-ADP binding to the strong nucleotide-binding site of the PriA helicase in buffer C (pH 7.0, 20 °C) containing 20 mM NaCl and 0.1 mM EDTA upon the total concentration of the enzyme. The solid lines are nonlinear least-squares fits according to the four-step sequential mechanism, defined by Scheme 1, with the equilibrium and rate constants: $K_1 = 5.0 \times 10^5$ M^{-1}, $k_2 = 170$ s^{-1}, $k_{-2} = 40$ s^{-1}, $k_3 = 5.1$ s^{-1}, $k_{-3} = 1.3$ s^{-1}, $k_4 = 0.125$ s^{-1}, and $k_{-4} = 0.025$ s^{-1} (details in text). (a) $1/\tau_2$. (b) $1/\tau_3$. (c) $1/\tau_4$. The error bars are standard deviations obtained from 3 to 4 independent experiments. (d) The dependence of the normalized relaxation amplitudes A_1, A_2, A_3, and A_4 for the binding of TNP-ADP to the PriA helicase in buffer C (pH 7.0, 20 °C) containing 20 mM NaCl and 0.1 mM EDTA upon the logarithm of the total enzyme concentration. The solid lines are nonlinear least-squares fits according to the four-step sequential mechanism, defined by Scheme 1, with the relative fluorescence intensities $F_{S_1} = 10$, $F_{S_2} = 21.6$, $F_{S_3} = 11.8$, and $F_{S_4} = 14.0$ (details in text). The rate constants are the same as in panels a−c: (■) A_1, (□) A_2, (●) A_3, and (○) A_4.

fluorescence intensity being a factor of ~12 larger for the ATP as compared to the ADP analogue (see the Discussion).

Kinetics of the TNP-ADP Binding to the Strong Nucleotide-Binding Site of the PriA Helicase in the Absence of Magnesium. Magnesium has a profound effect on the ADP and ATP analogue binding, particularly to the strong nucleotide binding sites of the PriA helicase (*67*). To address the role of magnesium in the dynamic of the cofactor binding to the strong nucleotide-binding site of the enzyme, we performed the analogous stopped-flow kinetic studies, as described above, in the absence of magnesium.

In the case of TNP-ADP, the fluorescence stopped-flow kinetic traces require three-exponential function to provide an adequate description of the experimental curves (data not shown). Nevertheless, the amplitude of the resolved normal modes of the reaction do not account for the total amplitude of the observed kinetics; that is, there is an additional fast process, characterized by a relaxation time, τ_1, too short to be resolved in stopped-flow experiments, which precedes the observed normal modes of the reaction (see above). The reciprocal relaxation times of the resolved normal modes $1/\tau_2$, $1/\tau_3$, and $1/\tau_4$ as a function of the total PriA concentration are shown in panels a−c of Figure 6. The plots indicate that all three relaxation times show little dependence on the protein concentration; thus, they characterize first-order transitions of the formed complex (*40*−*46*, *53*, *54*). The presence of the fast, unresolved process and the behavior of the relaxation times are analogous to the behavior observed in the presence of magnesium (Figure 3). Therefore, in the absence of magnesium, the binding of the ADP analogue is described by the same four-step sequential mechanism as depicted in Scheme 1. In other words, the absence of Mg^{2+} in solution does not affect the mechanism of the ADP analogue binding to the strong nucleotide-binding site, although it dramatically changes the dynamics and energetics of the partial reactions (see below). The dependence of the normalized amplitudes A_1, A_2, A_3, and A_4 upon the PriA concentration is shown in Figure 6d. Although amplitude A_2 still has the largest value, the amplitude A_1 of the fast unresolved process is comparable to A_2 and has a large contribution to the observed relaxation process over the entire range of the protein concentrations. Also, the amplitude A_3 now has much larger negative values as compared to the same parameter obtained in the presence of Mg^{2+} (Figure 3d). Only amplitude A_4 of the slowest relaxation mode is similar to the amplitude of the same normal mode determined in the presence of Mg^{2+}.

The analysis of the relaxation times and amplitudes has been performed in an analogous way as described above (Figure 3). Here we used the fact that the intrinsic binding constant $K_{B_1} = 5.1 \times 10^7$ M^{-1} (*67*) and the maximum, fractional increase of the ADP analogue fluorescence, $\Delta F_{1_{max}} = 12.0 \pm 0.3$, are known from the independent equilibrium titration experiment similar to the ones performed in the presence of magnesium (Figure 1) (data not shown). Moreover, these quantities are analytically defined in terms of

the partial equilibrium, rate, and spectroscopic parameters by eqs 9 and 10. The obtained rate, equilibrium, and relative molar fluorescence parameters are included in Table 1.

In the absence of magnesium, the formation of the $(S)_1$ intermediate in the nucleoside diphosphate binding to the strong nucleotide-binding site of the PriA helicase becomes energetically more favorable, with the partial equilibrium constant K_1 increased by a factor of ~5. However, the forward rate constant k_2 for the following transition $(S)_1 \leftrightarrow (S)_2$ decreases from 300 ± 50 s^{-1} to 170 ± 30 s^{-1}, while the backward rate constant k_{-2} increases by a factor of 2. As a result, the value of K_2 decreases from 15 ± 5 to 4.3 ± 1.5. The most dramatic effect is observed for the $(S)_3$ and $(S)_4$ intermediates. The partial equilibrium constants K_3 and K_4 increase by a factor of ~30 and ~10, from 0.13 ± 0.04 and 0.50 ± 0.15 to 3.9 ± 0.9 and 5.0 ± 1.4, respectively, predominantly through the large decrease of the backward rate constants k_{-3} and k_{-4}. The absence of magnesium in solution destabilizes the $(S)_1$ intermediate and strongly stabilizes the $(S)_3$ and $(S)_4$ intermediates (Table 1). Therefore, in the absence of Mg^{2+}, all first-order transitions in the ADP analogue binding to the strong nucleotide-binding site are energetically favorable, resulting in the overall binding constant, K_{B_1}, increased by a factor of ~33. Changes in the energetics of the formed intermediates are also accompanied by changes in their relative molar fluorescence intensities. Both F_{S_1} and F_{S_2}, characterizing the $(S)_1$ and $(S)_2$ intermediates, increase by a factor of ~2, while the relative molar intensity of the $(S)_3$ intermediate undergoes the largest increase from 1.3 ± 0.3 to 20.2 ± 0.4 (Table 1). On the other hand, the molar fluorescence intensity of the $(S)_4$ is decreased in the absence of magnesium (see the Discussion).

Kinetics of the TNP-ATP Binding to the Strong Nucleotide-Binding Site of the PriA Helicase in the Absence of Magnesium. To address the role of magnesium in the dynamics and energetics of the nucleoside triphosphate binding to the strong nucleotide-binding site of the PriA helicase, corresponding fluorescence stopped-flow studies have been performed with TNP-ATP. As observed in the presence of Mg^{2+}, kinetic traces are described by two-exponential function and an additional fast process characterized by a relaxation time τ_1, which is too short to be resolved in the stopped-flow experiments (*44*−*46*, *53*, *54*). The reciprocal relaxation times $1/\tau_2$ and $1/\tau_3$ as a function of the total PriA concentration are shown in panels a and b of Figure 7. The behavior of the relaxation times indicates that they characterize first-order transitions of the formed complex (see above) (*44*−*46*, *53*, *54*). Therefore, in the absence of magnesium, the binding of the nucleoside tri-phosphate is described by the same three-step sequential mechanism as depicted in Scheme 2.

The dependence of the normalized amplitudes A_1, A_2, and A_3 upon the PriA concentration is shown in Figure 7c. The dominant contribution of the amplitude A_2 to the observed relaxation process is preserved (Figure 5c); however, the amplitude A_1 of the fast, unresolved process has a very large contribution to the total amplitude. Moreover, it shows a much less pronounced dependence upon the protein concentration over the examined [PriA] range as compared to its behavior in the presence of Mg^{2+} (Figure 5c). Also, the amplitude A_3 shows little dependence upon the enzyme concentration, and it has large and negative values. The solid lines in Figure 7 are nonlinear least-squares fits of the relaxation times and amplitudes according to the mechanism defined by Scheme 2, using a single set of rate and spectroscopic parameters, performed in an analogous way as described above. This analysis is facilitated by the determination of the intrinsic binding constant $K_{B_1} = 1 \times 10^8$ M^{-1} (*67*) and the maximum, fractional increase of the ATP analogue fluorescence, $\Delta F_{1_{max}} = 12.4 \pm 0.3$, in the independent equilibrium titration experiment (data not shown).

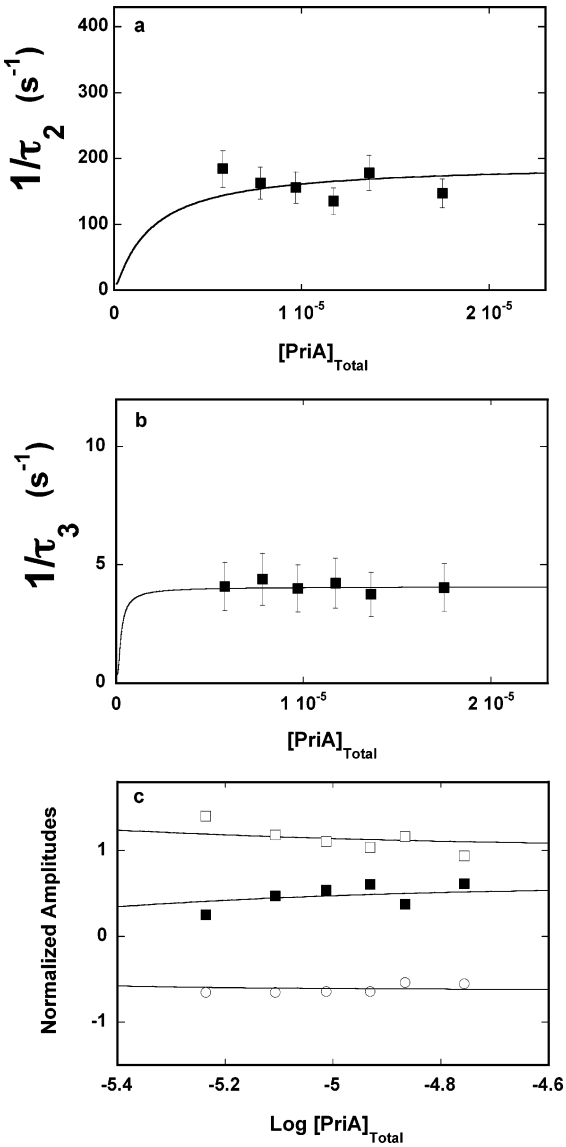

FIGURE 7: Dependence of the reciprocal relaxation times for the binding of TNP-ATP to the strong nucleotide-binding site of the PriA helicase in buffer C (pH 7.0, 20 °C) containing 20 mM NaCl and 0.1 mM EDTA upon the total concentration of the enzyme. The solid lines are nonlinear least-squares fits according to the three-step sequential mechanism, defined by Scheme 2, with the equilibrium and rate constants: $K_1 = 5.0 \times 10^5$ M^{-1}, $k_2 = 88$ s^{-1}, $k_{-2} = 5$ s^{-1}, $k_3 = 4$ s^{-1}, and $k_{-3} = 0.3$ s^{-1} (details in text). (a) $1/\tau_2$. (b) $1/\tau_3$. The error bars are standard deviations obtained from 3 to 4 independent experiments. (c) The dependence of the normalized relaxation amplitudes A_1, A_2, and A_3 for the binding of TNP-ATP to the PriA helicase in buffer C (pH 7.0, 20 °C) containing 20 mM NaCl and 0.1 mM EDTA upon the logarithm of the total enzyme concentration. The solid lines are nonlinear least-squares fits according to the three-step sequential mechanism, defined by Scheme 2, with the relative fluorescence intensities $F_{S_1} = 6.3$, $F_{S_2} = 16.8$, and $F_{S_3} = 10.1$ (details in text): (■) A_1, (□) A_2, and (●) A_3.

The obtained rate, equilibrium, and relative molar fluorescence parameters are included in Table 1.

Similar to the nucleoside diphosphate binding in the absence of magnesium the formation of the $(S)_1$ intermediate in the triphosphate analogue binding becomes energetically more favorable (Table 1). In contrast, the forward rate constant k_2 of the following transition, $(S)_1 \leftrightarrow (S)_2$, decreases significantly from 580 ± 70 s^{-1} to 88 ± 20 s^{-1} while the backward rate constant k_{-2} decreases only by a factor of 3, resulting in a decreased value of K_2 by a factor of ~2. However, the most dramatic effect is observed for the formation of the $(S)_3$ intermediate. The partial equilibrium constants K_3 increases by a factor of ~150 from 0.09 ± 0.04 to 13.3 ± 4.3, predominantly through the decrease of the backward rate constants k_{-3}. Therefore, the absence of magnesium stabilizes the $(S)_1$ intermediate, slightly destabilizes the following $(S)_2$ intermediate but very strongly stabilizes the $(S)_3$ intermediates (Table 1). Nevertheless, all first-order transitions in the nucleoside triphosphate binding to the strong nucleotide-binding site are energetically favorable, resulting in the overall binding constant, K_{B_1}, increased by a factor of ~23. Unlike the magnesium effect on the relative fluorescence intensities of the nucleoside diphosphate intermediates, the relative molar fluorescence intensities of the intermediates of the ATP analogue are less affected by the absence of Mg^{2+} (see the Discussion).

Kinetics of Binding of the TNP-ADP and TNP-ATP Analogue to the Weak Nucleotide-Binding Site of the PriA Helicase. The kinetic studies discussed so far focused on the dynamics of the nucleotide cofactor binding to the strong nucleotide-binding site of the PriA helicase. In the subsequent set of experiments, we examined the kinetics of the analogue binding to the weak nucleotide-binding site of the PriA helicase. Recall, we could examine exclusively the interactions with the strong binding site because its affinity is approximately 2 orders of magnitude higher than the affinity of the weak site (*67*). The same difference in affinities allows us to access the weak nucleotide-binding site independent of the events in the strong binding site.

To accomplish that, we used the following experimental design. The PriA helicase is premixed with the nucleotide analogue at a concentration of the cofactor, high enough to exclusively saturate only the strong binding site, for example, [nucleotide analog] ≤ 1 × 10^{-5} M, and allowed to reach the equilibrium. If this premixed system, which contains the helicase having only weak binding site still available for the cofactor, is subsequently mixed with the identical concentration of the cofactor (1 × 10^{-5} M) no relaxation effect should be observed because the strong site is saturated with the cofactor and the affinity of the weak site is too low to detectably engage in interactions with the cofactor. However, if the premixed system is mixed with the nucleotide analogue at a concentration of the cofactor that is high enough to bind to the weak site, the relaxation process of the cofactor binding to the weak nucleotide-binding site should be observed.

The fluorescence stopped-flow kinetic trace after mixing a solution containing 2 × 10^{-6} M PriA and 1 × 10^{-5} M TNP-ADP with 1 × 10^{-5} M TNP-ADP (final concentrations) in buffer C (pH 7.0, 20 °C) containing 20 mM NaCl and 5 mM $MgCl_2$ is shown in Figure 8a. The experimental trace is a straight line indicating, as expected, the absence of any relaxation process (see above). The fluorescence stopped-flow kinetic trace after mixing the same solution containing PriA and TNP-ADP, 2 × 10^{-6} M and 1 × 10^{-5} M, respectively, with 5 × 10^{-5} M TNP-ADP (final concentrations) is shown in Figure 8b. The concentration of the cofactor is now high enough to engage in interaction a significant fraction of the weak nucleotide-binding site (*67*). A relaxation process is observed that reflects the binding of the nucleoside diphosphate to the weak site of the PriA helicase. The solid line in Figure 8b is a nonlinear least-squares fit of the experimental curve using a one-exponential function (eq 1). Using a larger number of exponents in the fitting function does not improve the statistics of the fit (data not shown). The zero line, which in this case is a sum of the fluorescence intensity of the premixed PriA−TNP-ADP complex and the TNP-ADP solution containing 5 × 10^{-5} M of the cofactor (i.e., the same sample in the absence of

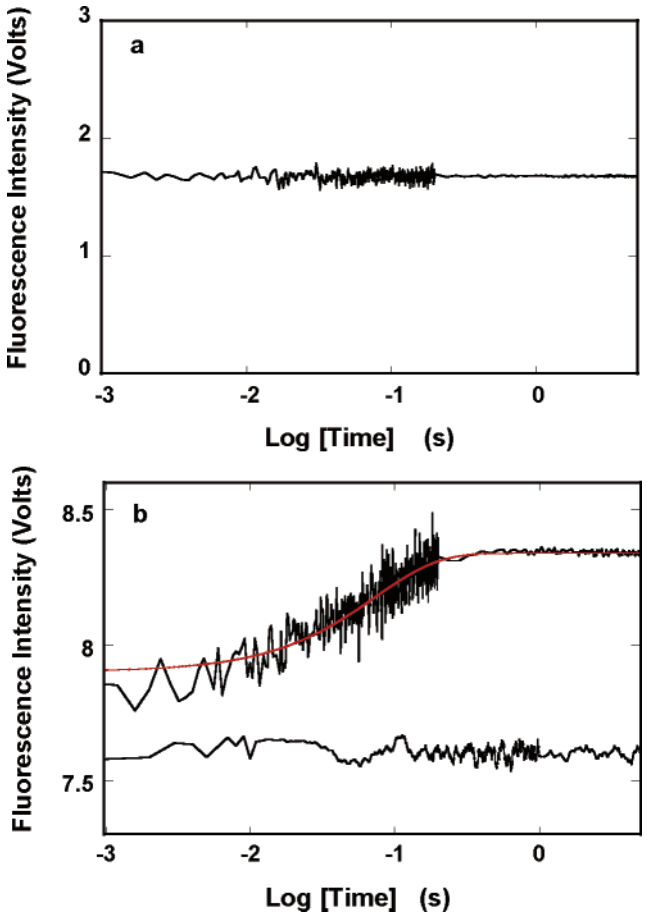

FIGURE 8: (a) Fluorescence stopped-flow kinetic trace after mixing the solution of TNP-ADP (1 × 10^{-5} M) with the solution containing PriA helicase and the same concentration of the cofactor in buffer C (pH 7.0, 20 °C) containing 20 mM NaCl and 5 mM $MgCl_2$ (λ_{ex} = 408 nm, λ_{em} > 500 nm). The final concentrations of the cofactor and the helicase are 2 × 10^{-6} M and 1 × 10^{-5} M, respectively. (b) Fluorescence stopped-flow kinetic trace after mixing the solution of TNP-ADP (9 × 10^{-5} M) with the solution containing PriA helicase and the cofactor (1 × 10^{-5} M), in buffer C (pH 7.0, 20 °C), containing 20 mM NaCl and 5 mM $MgCl_2$ (λ_{ex} = 408 nm, λ_{em} > 500 nm). The final concentrations of the helicase and the cofactor are 2 × 10^{-6} M and 5 × 10^{-5} M, respectively. The experimental kinetic trace is shown in logarithmic scale with respect to time. The horizontal part of the trace is the steady-state value of the fluorescence of the sample recorded 2 ms before the flow stopped (Materials and Methods). The solid line is the single-exponential, nonlinear least-squares fit of the experimental curve using eq 1.

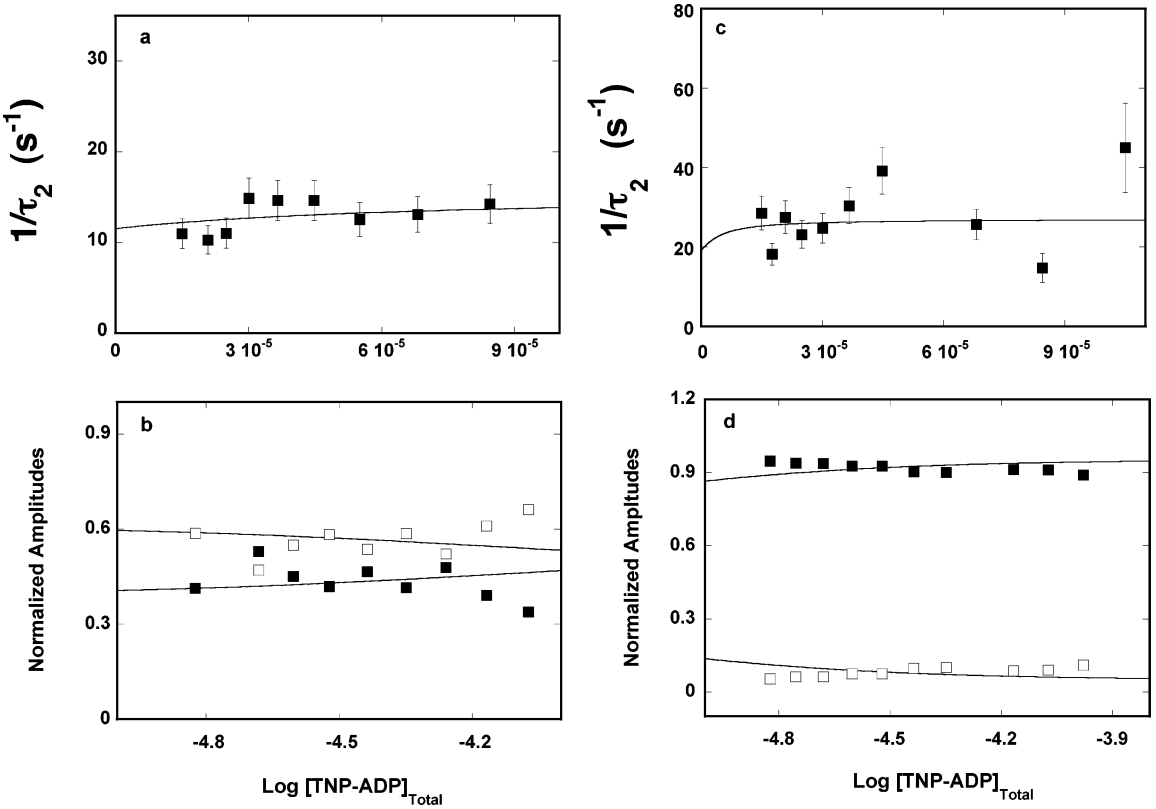

FIGURE 9: (a) Dependence of the reciprocal relaxation time, $1/\tau_2$, for the binding of TNP-ADP to the weak nucleotide-binding site of the PriA helicase in buffer C (pH 7.0, 20 °C) containing 20 mM NaCl and 5 mM $MgCl_2$ upon the total concentration of the cofactor. The solid line is the nonlinear least-squares fits according to the two-step sequential mechanism, defined by Scheme 3, with the equilibrium and rate constants: $K_1 = 1.4 \times 10^4$ M^{-1}, $k_2 = 4$ s^{-1}, and $k_{-2} = 11.5$ s^{-1} (details in text). (b) The dependence of the normalized relaxation amplitudes A_1 and A_2 for the binding of TNP-ADP to the weak nucleotide-binding sites of the PriA helicase in buffer C (pH 7.0, 20 °C) containing 20 mM NaCl and 5 mM $MgCl_2$ upon the logarithm of the total enzyme concentration. The solid lines are nonlinear least-squares fits according to the two-step sequential mechanism, defined by Scheme 3, with the relative fluorescence intensities $F_{W_1} = 3.1$ and $F_{W_2} = 10.6$. The maximum cofactor fluorescence increase is taken from the equilibrium fluorescence titration in the same solution conditions as $\Delta F_{2_{max}} = 4.3$ (details in text): (■) A_1 and (□) A_2. (c) The dependence of the reciprocal relaxation time, $1/\tau_2$, for the binding TNP-ADP to the weak nucleotide-binding site of the PriA helicase in buffer C (pH 7.0, 20 °C) containing 20 mM NaCl and 0.1 mM EDTA upon the total concentration of the cofactor. The solid line is the nonlinear least-squares fit according to the two-step sequential mechanism, defined by Scheme 3, with the equilibrium and rate constants: $K_1 = 1.4 \times 10^4$ M^{-1}, $k_2 = 4$ s^{-1}, and $k_{-2} = 11.5$ s^{-1} (details in text). (d) The dependence of the normalized relaxation amplitudes A_1 and A_2 for the binding of TNP-ADP to the weak nucleotide-binding sites of the PriA helicase in buffer C (pH 7.0, 20 °C) containing 20 mM NaCl and 0.1 mM EDTA upon the logarithm of the total enzyme concentration. The solid lines are nonlinear least-squares fits according to the two-step sequential mechanism, defined by Scheme 3, with the relative fluorescence intensities $F_{W_1} = 1.3$ and $F_{W_2} = 1.4$. The maximum cofactor fluorescence increase is taken from the equilibrium fluorescence titration in the same solution conditions as $\Delta F_{2_{max}} = 0.3$ (details in text): (■) A_1 and (□) A_2.

Scheme 3

$$(\mathbf{PriA})_W + \mathbf{D} \underset{k_{-1}}{\overset{k_1}{\leftrightarrow}} (\mathbf{W})_1 \underset{k_{-2}}{\overset{k_2}{\leftrightarrow}} (\mathbf{W})_2$$

the relaxation process) is also shown in Figure 8b. Clearly, the single-exponential fit does not account for the total amplitude of the reaction, indicating that an additional fast step precedes the observed relaxation processes (see above).

The dependence of the reciprocal relaxation time reaction $1/\tau_2$ extracted from the stopped-flow traces as a function of the total TNP-ADP concentration is shown in Figure 9a. The values of $1/\tau_2$ only slightly depend on the cofactor concentration, indicating that the relaxation time characterizes an intramolecular transition. The simplest mechanism that can account for the observed behavior of the relaxation times and the presence of the fast, unresolved step is a two-step sequential reaction described by Scheme 3. In other words, binding of nucleoside diphosphate to the weak nucleotide-binding site of the PriA helicase, in the presence of magnesium, is described by a simpler two-step mechanism as compared to the binding to the strong nucleotide-binding site that occurs in four sequential steps (Scheme 1). The dependence of the normalized individual amplitudes A_1 and A_2 is shown in Figure 9b. The amplitude of the fast unresolved mode, A_1, has been obtained in an analogous way as described for the TNP-ADP case from the known amplitude of the second normal mode, A_2, and the total amplitude of the reaction, A_T, as

$$A_1 = A_T - A_2 \tag{13}$$

The amplitude A_2 of the resolved normal mode has larger values than the amplitude A_1 of the fast bimolecular step, although A_2 does not have a dominant contribution to the overall relaxation process, as observed for the binding of the ADP cofactor to the strong nucleotide-binding site (Figure 3d). Both amplitudes show little dependence upon the cofactor concentration, in the examined [TNP-ADP] range.

The solid lines in Figure 9 are nonlinear least-squares fits of the relaxation times and amplitudes according to the mechanism defined by Scheme 3, using a single set of the

binding and rate parameters, K_1, k_2, and k_{-2}, and spectroscopic parameters, F_{W_1} and F_{W_2}. The parameters F_{W_1} and F_{W_2} are the relative molar fluorescence intensities of the nucleoside diphosphate cofactor in the first, $(W)_1$, and second, $(W)_2$, intermediate in the association reaction with the weak nucleotide-binding site of the PriA helicase. The fitting has been facilitated by the fact that the intrinsic binding constant $K_{B_2} = (1.9 \pm 0.6) \times 10^4\ M^{-1}$ and the maximum, fractional increase of the ADP analogue fluorescence, $\Delta F_{2_{max}} = 4.3 \pm 0.3$, are known from the independent equilibrium titration experiment (Figure 1). These quantities are analytically defined in terms of the partial equilibrium, rate, and spectroscopic parameters by

$$K_{B_2} = K_1(1 + K_2) \tag{14}$$

and

$$\Delta F_{2_{max}} = \frac{\Delta F_{W_1} + K_2 \Delta F_{W_2}}{Z_{D_2}} \tag{15}$$

where $K_1 = k_1/k_{-1}$ is the partial equilibrium constant characterizing the fast bimolecular step, $K_2 = k_2/k_{-2}$, $Z_{D_2} = 1 + K_2$, $\Delta F_{W_1} = (F_{W_1} - F_F)/F_F$, and $\Delta F_{W_2} = (F_{W_2} - F_F)/F_F$.

The bimolecular step in the ADP analogue binding to the weak site (Scheme 3) is very fast, similar to the same step in the binding to the strong site (Tables 1 and 2). The low affinity of the weak nucleotide-binding site is already generated at the bimolecular step (Scheme 3), which is characterized by $K_1 \approx 1.4 \times 10^4\ M^{-1}$ (i.e., approximately 1 order of magnitude lower value than the corresponding parameter for the strong binding site). If the forward rate constants k_1 were similar for both sites, then such a low value of K_1 would indicate a much larger value of k^{-1} and, in turn, a much shorter lifetime of the $(W)_1$ as compared to the $(S)_1$ intermediate. The formation of the $(W)_2$ intermediate with $k_2 = 4 \pm 1.1\ s^{-1}$ is dramatically slower as compared to the formation of $(S)_2$ ($k_2 \approx 300\ s^{-1}$), although the backward rate constant $k_{-2} = 11.5 \pm 3$ is similar (Table 1). As a result, the transition $(W)_1 \leftrightarrow (W)_2$ has the partial equilibrium constant $K_2 \approx 0.35$ and contributes negatively to the total free energy of binding. The value of the relative molar fluorescence intensity F_{W_1} of the $(W)_1$ intermediate (3.1 ± 0.5) is significantly lower than the value (5.1 ± 0.3) of F_{S_1} that characterizes the corresponding intermediate, $(S)_1$, in the binding of the ADP analogue to the strong binding site (Tables 1 and 2). However, the value of the relative molar fluorescence intensity, F_{W_2}, of the subsequent $(W)_2$ intermediate is very similar to the molar fluorescence intensity determined for the $(S)_2$ species (see the Discussion).

The absence of magnesium does not affect the mechanism of the ADP analogue binding to the weak nucleotide-binding site, which is still described by the two-step mechanism defined by Scheme 3 (data not shown). The dependence of the reciprocal relaxation time reaction $1/\tau_2$ and the amplitudes extracted from the stopped-flow traces upon the total TNP-ADP concentration are shown in Figure 9, panels c and d. The solid lines in panels c and d of Figure 9 are nonlinear least-squares fits of the relaxation times and amplitudes, with a single set of the binding and rate parameters, K_1, k_2, and k_{-2}, and spectroscopic parameters, F_{W_1} and F_{W_2}, and using the intrinsic binding constant $K_{B_2} = (3.7 \pm 1.1) \times 10^5\ M^{-1}$

Table 2: Kinetic, Thermodynamic, and Spectroscopic Parameters Characterizing the Binding of TNP-ADP and TNP-ATP to the Weak Nucleotide-Binding Site of the *E. coli* PriA Helicase in Buffer C (pH 7.0, 20 °C) Containing 20 mM NaCl and 5 mM $MgCl_2$ or 0.1 mM EDTA

buffer	k_2 (s^{-1})	k_{-2} (s^{-1})	k_3 (s^{-1})	k_{-3} (s^{-1})	K_1 (M^{-1})	K_2	K_3	overall binding constant (M^{-1})	F_{W_1}	F_{W_2}	F_{W_3}	$F_{2_{max}}$
						TNP-ADP						
C 5 mM $MgCl_2$	4 ± 1	11 ± 3			$(1.4 \pm 0.5) \times 10^4$	0.35 ± 0.20		$(1.9 \pm 0.6) \times 10^4$	3.1 ± 0.5	10.6 ± 0.7		4.3 ± 1.5
C 0.1 mM EDTA	8 ± 2	19.0 ± 3.5			$(2.6 \pm 0.5) \times 10^5$	0.42 ± 0.19		$(3.7 \pm 2.1) \times 10^5$	1.3 ± 0.05	1.4 ± 0.05		0.3 ± 0.1
						TNP-ATP						
C 0.1 mM EDTA	1.1 ± 0.2	14.0 ± 3.5	0.15 ± 0.03	0.32 ± 0.08	$(7.1 \pm 0.4) \times 10^5$	0.08 ± 0.04	0.47 ± 0.20	$(7.9 \pm 2.5) \times 10^5$	1.31 ± 0.05	1.63 ± 0.05	0.92 ± 0.05	0.3 ± 0.1

Scheme 4

$$(\mathbf{PriA})_{\mathbf{W}} + \mathbf{T} \underset{\mathbf{k_{-1}}}{\overset{\mathbf{k_1}}{\leftrightarrow}} (\mathbf{W})_1 \underset{\mathbf{k_{-2}}}{\overset{\mathbf{k_2}}{\leftrightarrow}} (\mathbf{W})_2 \underset{\mathbf{k_{-3}}}{\overset{\mathbf{k_3}}{\leftrightarrow}} (\mathbf{W})_3$$

(*67*) and the maximum fractional increase of the ADP analogue fluorescence, $\Delta F_{2_{max}} = 0.3 \pm 0.1$, obtained from an independent equilibrium titration experiment (data not shown). These quantities are analytically defined in terms of the partial equilibrium, rate, and spectroscopic parameters by eqs 14 and 15.

In the absence of magnesium, the value of the partial equilibrium constant K_1 characterizing the bimolecular step (Scheme 3) increases by a factor of ~19. This is a much larger increase than observed for the corresponding parameter in the ADP analogue binding to the strong site (Tables 1 and 2). In fact, the entire increase of the overall binding constant, K_{B_2}, in the absence of magnesium, is generated at the bimolecular step through the increase of K_1, while the value of $K_2 = 0.42 \pm 0.18$ remains within experimental accuracy unaffected (Table 2). Nevertheless, the second step still contributes negatively to the overall free energy of binding to the weak site. The absence of Mg^{2+} cations also significantly affects the structure of the formed complex at the weak nucleotide-binding site. The relative molar fluorescence intensities of the $(W)_1$ and $(W)_2$ intermediates decrease dramatically and are only slightly higher than the emission of the free cofactor (Table 2). Such low values of the emission of the intermediates reflect the very low value of $\Delta F_{2_{max}} \approx 0.3$, characterizing the binding of the ADP analogue to the weak site, in the absence of Mg^{2+} (see above and the Discussion).

The kinetics of the ATP analogue binding to the weak nucleotide-binding site of the PriA helicase could only be examined in the absence of magnesium, which hinders the efficient hydrolysis of the cofactor by the enzyme (*67*). Stopped-flow data indicate that the association reaction with the weak binding site is described by a fast, unresolved step followed by two relaxation processes (data not shown). The dependence of the reciprocal relaxation times $1/\tau_2$ and $1/\tau_3$ extracted from the stopped-flow traces upon the total TNP-ATP concentration is shown in panels a and b of Figure 10. Both relaxation times are, within experimental accuracy, independent of the cofactor concentration, indicating that they characterize an intramolecular transition (*40*−*46*, *53*, *54*). The simplest mechanism, which can account for the observed behavior, is that, unlike the ADP analogue binding, the association reaction of TNP-ATP proceeds in a three-step sequential mechanism as defined by Scheme 4. The dependence of the normalized individual amplitudes A_1, A_2, and A_3 upon the cofactor concentration is shown in Figure 10c. The solid lines in Figure 10 are nonlinear least-squares fits of the relaxation times and amplitudes according to the mechanism defined by Scheme 4, performed as described above and utilizing the fact that the intrinsic binding constant $K_{B_2} \approx (7.8 \pm 0.8) \times 10^5\ M^{-1}$ (*67*) and the maximum, fractional increase of the TNP-ATP fluorescence in the weak binding site, $\Delta F_{2_{max}} = 0.3 \pm 0.1$, has been obtained in an independent equilibrium titration experiments (data not shown). These quantities are related to the partial reactions by

$$K_{B_2} = K_1(1 + K_2 + K_2K_3) \quad (16)$$

and

$$\Delta F_{2_{max}} = \frac{\Delta F_{W_1} + K_2\Delta F_{W_2} + K_3\Delta F_{W_3}}{Z_{T_2}} \quad (17)$$

where $Z_{T_2} = 1 + K_2 + K_2K_3$, and the remaining parameters have the same meaning as discussed for eqs 14 and 15. The plots in panels a−c of Figure 10 are generated using a single set of the binding, rate, and spectroscopic parameters (K_1, k_2, k_{-2}, F_{W_1}, F_{W_2}, and F_{W_3}) included in Table 2.

Similar to the ADP analogue, the bimolecular step in the ATP analogue binding to the weak nucleotide-binding site with the partial equilibrium constant, $K_1 \approx 7.1 \times 10^5\ M^{-1}$, completely dominates the overall free energy of binding, $\Delta G°$ ($K_{B_2} \approx 7.8 \times 10^5\ M^{-1}$). The $(W)_1 \leftrightarrow (W)_2$ and $(W)_2 \leftrightarrow (W)_3$ transition are characterized by the partial equilibrium constants $K_1 \approx 0.08$ and $K_2 \approx 0.47$, respectively (i.e., they contribute negatively to $\Delta G°$). Also, the values of the relative molar fluorescence intensities of all intermediates are only slightly higher than the emission intensity of the free cofactor (Table 2). As observed for TNP-ADP, the low values of fluorescence intensities of the intermediates reflect the very low value of $\Delta F_{2_{max}} \approx 0.3$, characterizing the binding of the ATP analogue to the weak nucleotide-binding site of the PriA helicase (see the Discussion).

DISCUSSION

Multiple-Step Kinetic Mechanisms of Nucleotide Binding to the Strong Nucleotide-Binding Site of the PriA Helicase in the Presence of Magnesium. The results obtained in this work indicate that the mechanisms of the nucleoside di- and triphosphate to the strong nucleotide-binding site of the PriA binding to the ssDNA are complex sequential processes described by Schemes 1 and 2. Thus, the enzyme−cofactor complexes undergo a series of conformational transitions following the initial bimolecular step. In the case of the ATP analogue, the bimolecular step is very fast beyond the resolution of the stopped-flow measurements. Such fast bimolecular step and the sequential nature of the mechanism indicate that the strong nucleotide-binding site is easily accessible to the cofactor and the site does not undergo any conformational adjustment prior to the nucleotide binding. On the other hand, the relative fluorescence increase, F_{S_1}, of the first intermediate, $(S)_1$, is ~5-fold larger than the fluorescence of the free cofactor in solution (Table 1). This significant increase of the analogue fluorescence, as compared to the free cofactor, accompanying the formation of the $(S)_1$ intermediate, argues against the notion that it is a simple collision complex (*55*, *56*). Rather, it must include a fast conformational change of the protein−cofactor complex occurring in the formation of $(S)_1$ that places the entire TNP moiety in a nonpolar environment (*33*, *35*, *36*, *50*, *51*).

The step following the bimolecular association (Schemes 1 and 2) is also fast and characterized by the forward rate constant, $k_2 \sim 580\ s^{-1}$. This value is higher than k_2 ~300 s^{-1} determined for the ADP analogue and strongly suggests that the interactions of the phosphate group is involved in the transition to $(S)_2$. This conclusion is further supported by the effect of magnesium on the kinetics of both ATP and

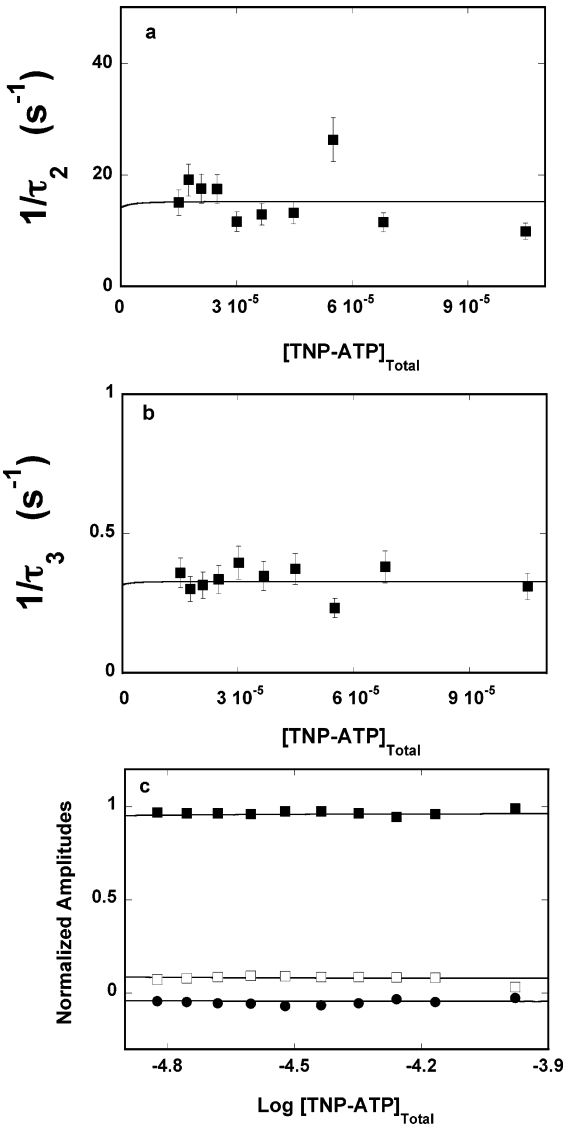

FIGURE 10: Dependence of the reciprocal relaxation times and for the binding of TNP-ATP to the weak nucleotide-binding site of the PriA helicase in buffer C (pH 7.0, 20 °C) containing 20 mM NaCl and 0.1 mM EDTA upon the total concentration of the cofactor. The solid lines are the nonlinear least-squares fits according to the three-step sequential mechanism, defined by Scheme 4, with the equilibrium and rate constants: $K_1 = 7.1 \times 10^5$ M^{-1}, $k_2 = 1.1$ s^{-1}, $k_{-2} = 14.0$ s^{-1}, $k_3 = 0.15$ s^{-1}, and $k_{-3} = 0.32$ s^{-1} (details in text). (a) $1/\tau_2$. (b) $1/\tau_3$. (c) The dependence of the normalized relaxation amplitudes A_1, A_2, and A_3 for the binding of TNP-ATP to the weak nucleotide-binding sites of the PriA helicase in buffer C (pH 7.0, 20 °C) containing 20 mM NaCl and 0.1 mM EDTA upon the logarithm of the total enzyme concentration. The solid lines are nonlinear least-squares fits according to the three-step sequential mechanism, defined by Scheme 4, with the relative fluorescence intensities $F_{W_1} = 1.31$, $F_{W_2} = 1.63$, and $F_{W_3} = 0.92$. The maximum cofactor fluorescence increase is taken from the equilibrium fluorescence titration in the same solution conditions as $\Delta F_{2_{max}} = 0.3$ (details in text): (■) A_1, (□) A_2, and (●) A_3.

ADP analogues binding (see below). On the other hand, the backward rate constant, k_{-2}, is in the range of ∼15−20 s^{-1} for both cofactors. Thus, the transition $(S)_1 \leftrightarrow (S)_2$ provides a strong additional stabilization of the protein−cofactor complex, albeit larger for the nucleoside triphosphate. Such a substantial and positive free energy change makes the $(S)_2$ intermediate a dominant species (see below) and, in light of efficient hydrolysis of the TNP-ATP by the PriA helicase, indicates that the $(S)_2$ intermediate is a part of the catalytic cycle of the ATP hydrolysis. The values of k_2 and k_{-2} indicate that, while the formation of the $(S)_2$ intermediate occurs in a couple of milliseconds, the lifetime of the intermediate is in the range of tens of milliseconds. Such a long lifetime would allow the intermediate to engage in different stages of catalysis in interactions with the DNA (*31*). The final transition, in the case of the triphosphate analogue, $(S)_2 \leftrightarrow (S)_3$, is very different from the $(S)_1 \leftrightarrow (S)_2$ step. It is slower by approximately 2 orders of magnitude. Moreover, it is characterized by a very low partial equilibrium constant $K_3 = 0.09 \pm 0.04$ (i.e., it is energetically unfavorable). In the context of the current estimates of the rate of the PriA helicase translocation on the DNA at about ∼90 nucleotides per second, the data strongly suggest that intermediates such as $(S)_3$ are not involved in the translocation and the catalysis of the dsDNA unwinding (*22*).

Amplitude analysis shows that, with each transition in the strong nucleotide-binding site, the relative molar fluorescence intensity of the bound TNP-ATP strongly increases with respect to the emission intensity of the free cofactor (Table 1). As we pointed out above, the fluorescence properties of TNP nucleotide analogues are very sensitive to the solvent polarity and are suitable to examine the cofactor-binding properties of nucleotide-binding enzymes as well as reporters of the physical nature of the binding site (*32*, *35*, *36*, *50*, *51*, *58*). We have previously used this property of the TNP analogue to examine the nature of the nucleotide binding to the *E. coli* replicative helicase DnaB protein (*35*, *36*). The emission intensity of the analogues strongly increases with the decreasing polarity of the environment and shows a very good correlation with the Kosower's empirical polarity *Z* scale (*59*). In this context, the obtained results indicate that with each transition, the nucleoside triphosphate is placed in a more and more hydrophobic environment (i.e., more and more separated from the solvent).

Kinetic Mechanism of the Nucleoside Diphosphate Binding to the Strong Nucleotide-Binding Site of the PriA Helicase Contains an Additional Intermediate as Compared to the Mechanism of the Nucleoside Triphosphate Binding: *The Exit Intermediate of the Hydrolysis Product.* Surprisingly, the kinetic mechanism of the nucleoside di-phosphate binding to the strong nucleotide-binding site is more complex than observed for the ATP analogue and contains an additional slow step (Scheme 1). Nevertheless, the first two steps are similar for both cofactors in terms of the rate constants and relative molar fluorescence intensities characterizing the $(S)_1$ and $(S)_2$ intermediates, indicating a similar orientation of the bound nucleotides and the structure of the formed complexes independent of the number of the phosphate groups. A dramatic difference occurs in the case of the $(S)_3$ intermediate. Although the dynamics of its formation is similar to the ATP analogue, the relative molar fluorescence intensity, $F_{S_3} = 1.3 \pm 0.1$, for example, is more than an order of magnitude lower than the $F_{S_3} = 15.6 \pm 0.3$ determined for TNP-ATP (Table 1). Actually, the relative value of ∼1.3 indicate that the emission of the $(S)_3$ intermediate in ADP analogue binding is barely different from the emission intensity of the free cofactor in solution. These results indicate that, unlike the nucleoside triphosphate, the ADP analogue in the strong binding site passes through an intermediate where it becomes completely accessible to the solvent (i.e., it leaves the

hydrophobic environment of the cleft of the binding site).

Notice, the more complex behavior of the nucleoside diphosphate in the strong nucleotide-binding site can be understood if one takes into account the fact that it is the hydrolysis product of ATP and the strong site is the dominant ATPase site of the enzyme (*67*). Unlike ATP, the nucleoside diphosphate must leave the binding site without undergoing any chemical change. In other words, there should be an intermediate(s) where the diphosphate cofactor moves toward the exit of the binding site, while a transition of that nature is not necessary for the triphosphate counterpart. This is what is experimentally observed here. On the other hand, the $(S)_3$ intermediate undergoes an additional transition to $(S)_4$, apparently not present in the case of the triphosphate analogue (Scheme 1 and 2). This intermediate has its molar fluorescence intensity, $F_{S_4} = 16.0 \pm 0.3$, virtually identical, within experimental accuracy, to the molar intensity, $F_{S_4} = 15.6 \pm 0.3$, of the final $(S)_3$ intermediate in the ATP analogue binding (Table 1). In the context of the discussion above, we can reassign the intermediate $(S)_3$ in the ATP analogue binding as physically corresponding to the $(S)_4$ intermediate in the ADP analogue binding. Therefore, what is different in the mechanism of the ATP analogue binding (Scheme 2) to the strong nucleotide-binding site as compared to the mechanism of the ADP analogue binding (Scheme 1) is not the absence of the $(S)_4$ intermediate, but rather the absence of the exit intermediate $(S)_3$ that would correspond to the $(S)_3$ intermediate in the ADP binding where the cofactor becomes exposed to the solvent.

Magnesium Cations Dramatically Affect the Distribution of the ATP and ADP Intermediates in the Strong Nucleotide-Binding Site of the PriA Helicase. Although Mg^{2+} cations do not affect the kinetic mechanisms of the ATP and ADP analogue binding to the strong nucleotide-binding site of the PriA helicase, as defined by Schemes 1 and 2, magnesium has a pronounced effect on rates and energetics of the partial reactions in both mechanisms. Interestingly, the transition $(S)_1 \leftrightarrow (S)_2$ is the least affected by magnesium for both the ATP and ADP analogue. The forward rate constant, k_2, increases in the presence of Mg^{2+}, particularly in the case of nucleoside triphosphate by a factor of ~6, while the backward rate constant, k_{-2}, is affected to a lesser extent. As a result, the partial equilibrium constant, K_2, moderately increases by a factor of ~2−3 for both cofactors (Table 1). However, the effect on the subsequent transitions is dramatic. In the case of the ATP analogue, the value of K_3 decreases from ~13.3 in the absence of magnesium to ~0.09 (i.e., by a factor of ~150) in the presence of 5 mM $MgCl_2$, predominantly due to the large increase of the backward rate constant k_{-3}. Analogous effect of magnesium is observed for the ADP analogue. The values of $K_3 \approx 3.9$ and $K_4 \approx 5.0$, characterizing transition $(S)_2 \leftrightarrow (S)_3$ and $(S)_3 \leftrightarrow (S)_4$ in the absence of magnesium, are reduced by a factor of ~30 and ~10, respectively, in the presence of Mg^{2+} cations, predominantly due to increases in the values of the backward rate constants k_{-3} and k_{-4}.

Such dramatic effect of magnesium on the rate and energetics of the partial steps in the binding of the ATP and ADP analogues to the strong nucleotide-binding site of the PriA helicase profoundly changes the distribution of populations of the intermediates. Figure 11a shows computer simulations of the dependence of the fractional populations of all three intermediates in the reaction of the triphosphate analogue binding to the strong site, in the absence of magnesium, upon the logarithm of the free concentration of the nucleotide. The fractional distribution has been calculated using the determined partial equilibrium parameters included in Table 1. In the [TNP-ATP] range, where the site becomes saturated with the cofactor ($>10^{-7}$ M), the last $(S)_3$ intermediate dominates the distribution, constituting ~92% of the total population of the bound cofactor. The fractional contribution of the $(S)_2$ intermediate reaches ~7% of the total population, while the $(S)_1$ intermediate has negligible contribution (<0.5%). The situation is very different in the presence of magnesium as depicted in Figure 11b. The $(S)_2$ intermediate is now a dominating species constituting ~90% of the total population, while intermediate $(S)_3$ is reduced to ~8% of the total population. The fractional population of the $(S)_1$ intermediate remains low, reaching the value of ~2%, in the presence of Mg^{2+}.

The dependence of the fractional populations of intermediates in the reaction of the ADP analogue binding to the strong nucleotide-binding site, in the absence of magnesium, upon the logarithm of the free concentration of TNP-ADP is shown in Figure 11c. At saturation, the $(S)_4$ intermediate dominates the distribution constituting ~79% of the total population of the bound cofactor. The fractional contribution of the $(S)_3$ intermediate reaches ~16%, while the $(S)_2$ intermediate has only ~4% contribution to the total population. The $(S)_1$ intermediate constitutes a negligible fraction of the total population. The presence of magnesium changes diametrically the distribution of the intermediates (Figure 11d). As observed for the ATP analogue, the $(S)_2$ intermediate is now a dominating species constituting ~80% of the total population, the $(S)_3$ intermediate is reduced to ~10% of the total population, while the $(S)_1$ and $(S)_4$ intermediates have very similar, approximately 5%, contributions to the population of the bound ADP analogue.

Thus, for both tri- and diphosphate cofactors, the $(S)_2$ intermediate becomes selected in the presence of magnesium as the dominant species in the strong nucleotide-binding site of the PriA helicase. Such behavior and the fact that the PriA helicase hydrolyzes TNP-ATP in the absence of the ssDNA, even more efficiently than the unmodified ATP, strongly support the conclusion that the $(S)_2$ intermediate is the major species in the ATP-catalytic cycle of the enzyme (see above). Recall, magnesium is catalytically necessary in the ATP hydrolysis catalyzed by an ATPase in facilitating the transfer of the γ-PO^{4-} group to water (*59*). The results discussed here indicate that magnesium can also strongly affect the efficiency of ATP hydrolysis by profoundly changing the populations of the different intermediates of the enzyme−cofactor complex. Thus, the population of the active $(S)_2$ intermediate in the TNP-ATP binding to the strong site increases by a factor of ~12 in the presence of Mg^{2+} (Figure 11). By the same token, the population of the nonproductive species $(S)_3$ in the ATP analogue binding is strongly diminished.

Notice, the population of the $(S)_3$ intermediate in the ADP analogue binding in the presence of Mg^{2+} cations is lower than in the absence of magnesium, nevertheless, it is still the second species in terms of the fractional contribution to the intermediate population. Therefore, a significant fraction of the bound nucleoside di-phosphate reaches the exit

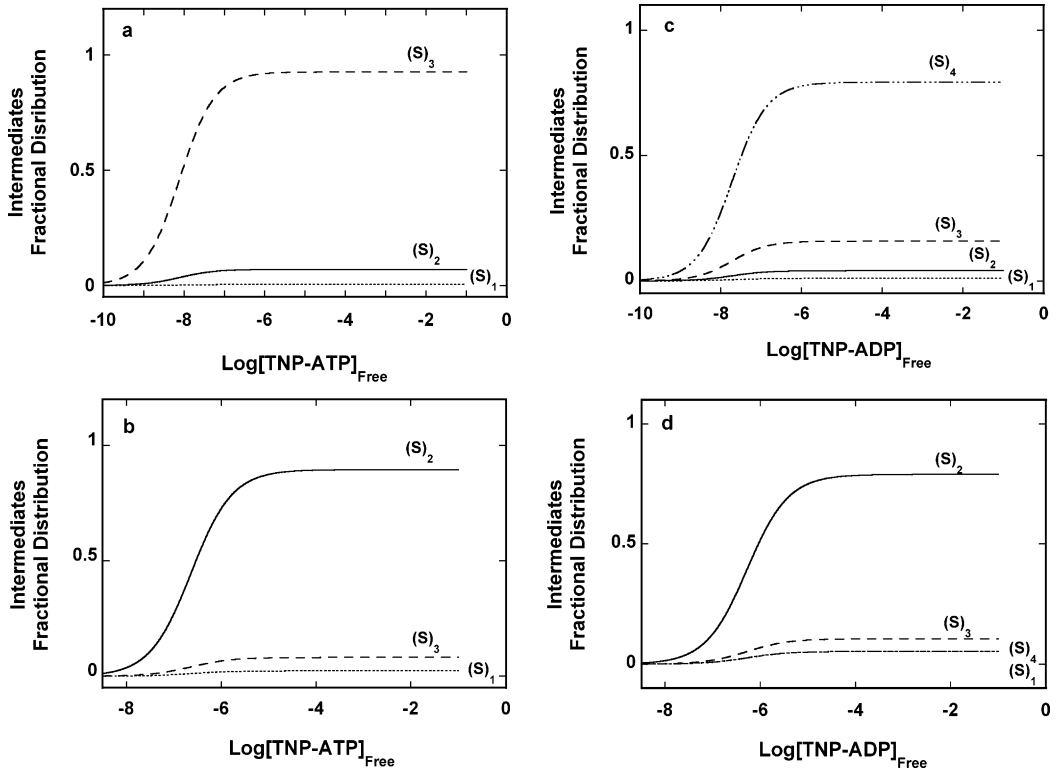

FIGURE 11: (a) Computer simulations of the dependence of fractional contributions of intermediates $(S)_1$, $(S)_2$, and $(S)_3$ for the mechanism (Scheme 2) of the ATP analogue 56 binding to the strong nucleotide-binding site of the PriA helicase, upon the logarithm of the free TNP-ATP concentration in the absence magnesium. The plots have been obtained using equilibrium and rate parameters obtained in the absence of Mg^{2+} included in Table 1: $(S)_1$ (---), $(S)_2$ (—), and $(S)_3$ (— —). (b) Computer simulations of the dependence of fractional contributions of intermediates in the ATP analogue binding to the strong nucleotide-binding site of the PriA helicase upon the logarithm of the free TNPATP concentration in the presence of magnesium. (c) Computer simulations of the dependence of fractional contributions of intermediates $(S)_1$, $(S)_2$, $(S)_3$, and $(S)_4$ for the mechanism (Scheme 1) of the ADP analogue binding to the strong nucleotide-binding site of the PriA helicase upon the logarithm of the free TNP-ADP concentration in the absence of magnesium. The plots have been obtained using equilibrium and rate parameters obtained in the absence of Mg^{2+} included in Table 1: $(S)_1$ (---), $(S)_2$ (—), $(S)_3$ (— —), and $(S)_4$ (—·---—). (d) Computer simulations of the dependence of fractional contributions of intermediates in the ADP analogue binding to the strong nucleotide-binding site of the PriA helicase, upon the logarithm of the free TNP-ADP concentration in the presence of magnesium (see text for details).

intermediate, although, controlled by Mg^{2+} binding. The magnesium effect on the dynamics and energetics of the formations of the individual intermediates is paralleled by the changes in their structures. This is particularly evident in the case of the ADP analogue where the relative molar fluorescence intensities of all first three intermediates, $(S)_1$, $(S)_2$, and particularly $(S)_3$ (Scheme 1), are significantly lower in the presence of Mg^{2+} (Table 1). Such behavior of the fluorescence of the bound TNP analogues indicates that, in the presence of Mg^{2+}, the cofactors are moved into a less hydrophobic environment, with the ADP cofactor being practically exposed to the solvent in the $(S)_3$ intermediate (*35*, *36*, *50*, *51*, *59*).

Intermediates in the Association of the Nucleoside Di- and Triphosphates with the Weak Nucleotide-Binding Site Are of a Very Different Nature as Compared to the Intermediates Formed at the Strong Binding Site. Equilibrium fluorescence studies provided the first indication that the complex formed at the weak nucleotide-binding site has a very different nature as compared with the complex formed at the strong binding site. Besides an approximately 2 orders of magnitude lower affinity, in the presence of magnesium, the relative maximum fluorescence increase of the TNP-ADP $\Delta F_{2_{max}} = 4.3 \pm 0.3$), that is, it is by a factor of ~2 lower than $\Delta F_{1_{max}} = 9.0 \pm 0.3$, observed for the strong binding site (Figure 1). An even lower value of $\Delta F_{2_{max}} \approx 0.3$ is observed in the absence of magnesium, which is barely detectable, while in the same conditions, $\Delta F_{1_{max}} \approx 12$ (Tables 1 and 2). A very similar difference between the spectroscopic parameters characterizing the two binding sites is also observed for the ATP analogue in the absence of magnesium. Thus, in the weak site, the nucleotide cofactor experiences a much less hydrophobic environment than in the strong site, independent of the number of the phosphate groups (see above) (*35*, *36*, *50*, *51*, *59*).

The kinetic mechanism of the ADP analogue binding to the weak nucleotide-binding site of the PriA helicase includes only two intermediates (Scheme 3) and is remarkably simpler than the mechanism of the same cofactor binding to the strong site, which includes four intermediates (Scheme 1). Moreover, the energetics and the nature of the formed intermediates are different from the intermediates in the association reaction with the strong site. This is observed both in the presence and absence of magnesium. Noticeably, the entire magnesium effect is expressed in the value of the partial equilibrium constant, K_1, instead of the energetics of the formation of intermediates following the bimolecular step as observed for the strong site, where magnesium stabilizes the $(S)_2$ species and destabilizes all remaining intermediates (Figure 11, see above). The $(W)_1 \leftrightarrow (W)_2$ transition is not shifted toward the $(W)_2$ species, as observed for the analogous $(S)_1 \leftrightarrow (S)_2$ transition in the strong binding site.

As a result, the bound ADP analogue exists in equilibrium between two intermediates, $(W)_1$ and $(W)_2$, in the presence or absence of magnesium, with $(W)_2$ species constituting ~30% of the total population of the bound cofactor at saturation.

Notice, in the case of the weak site, the value of K_1 decreases by a factor of ~19 in the presence of magnesium, while it decreases only by a factor of ~5 in the strong binding site. This difference indicates that different regions of the cofactor are engaged in interactions in two sites, even in the bimolecular binding step (see below and ref *67*). However, magnesium does affect the structure of the helicase−cofactor complex in the weak site, as expressed by large increases of the relative molar fluorescence intensities F_{W_1} and F_{W_2} in the presence of Mg^{2+} (Tables 1 and 2). Nevertheless, the value of F_{W_1} is significantly lower than the corresponding value of F_{S_1}, indicating that the cofactor is more exposed to the solvent in the dominant intermediate in the weak site than in the strong site. In fact, in the absence of Mg^{2+}, the values of F_{W_1} and F_{W_2} are barely different from the emission intensity of the free cofactor, indicating that the nucleotide is very close to the protein surface, while in the strong site in the absence of Mg^{2+} the nucleotide is placed in an even more hydrophobic environment than in the presence of Mg^{2+}.

Unlike the ADP analogue, the kinetic mechanism of the ATP analogue binding to the weak nucleotide-binding site is a three-step sequential mechanism, that is, the same as observed for the ATP analogue binding to the strong binding site (Schemes 2 and 4). However, the similarity ends here. Although the kinetics could not be examined in the presence of magnesium, the fact that the Mg^{2+} cations little affect the ADP analogue binding strongly suggests that the behavior observed in the absence of magnesium, for the TNP-ATP, will also be observed in the presence of Mg^{2+} (Table 2). The $(W)_1$ species is the dominant intermediate, while the $(W)_1 \leftrightarrow (W)_2$ and $(W)_2 \leftrightarrow (W)_3$ transitions have both negative contributions to the overall free energy of binding. In contrast, in the ATP analogue association with the strong binding site, in the absence of magnesium, the corresponding transitions contribute significantly and positively to $\Delta G°$ (Tables 1 and 2). The relative molar fluorescence intensities of all intermediates are close to the fluorescence intensity of the free cofactor, indicating that the cofactor is located close to the surface of the protein and in significant contact with the solvent (Table 2). On the other hand, in the strong site, all relative molar fluorescence intensities are high, indicating a strongly hydrophobic environment with little contact with the bulk solvent of the ATP analogue in all intermediates (Table 1).

The Weak Nucleotide-Binding Site of the PriA Helicase May Have an Allosteric Control Role in the Activities of the Enzyme. The affinity of the weak nucleotide-binding site shows only slight dependence on the type of the base, indicating the lack of specific short range interactions with the base, predominantly involving interactions with the variant of the phosphate binding loop, located in the helicase motif VI of the PriA helicase (*66*, *67*). Such structure of the weak nucleotide-binding site would corroborate well with the observed lack of the base specificity, a simpler kinetic mechanism of ADP analogue binding, and the properties of the kinetic intermediates. A conspicuous feature of the ADP analogue binding to the weak site is the effect of the of magnesium on the internal energetics of the intermediates and the absence of an intermediate corresponding to the exit intermediate $(S)_3$ in the strong site. Magnesium exerts strong effect only on the partial equilibrium binding constant K_1 in the TNP-ADP binding to the weak binding site, as opposed to only a moderate effect on the analogous parameter for the strong site, strongly suggesting that the initial association with the weak site occurs through interactions between the positively charged groups of the site and the phosphate group, partially neutralized in the presence of Mg^{2+}. On the other hand, the internal energetics between the intermediates is not affected by Mg^{2+}. These results strongly suggest that the weak site participates in different pathways of interactions as compared to the strong site (*67*, *68*).

There are also significant differences between the ADP and ATP analogue complexes with the weak nucleotide-binding site, suggesting a different function of the nucleoside di- and triphosphate bound in the weak site (*68*). Thus, the bound ADP cofactor in the weak site is in equilibrium between two intermediates, $(W)_1$ and $(W)_2$, with $(W)_2$ constituting a large fraction of the population of the bound cofactor. Binding of the ATP analogue includes three steps, and the $(W)_1$ intermediate completely dominates the intermediate distribution with $(W)_2$ and $(W)_3$ constituting only ~7% and ~4% of the population of the bound cofactor, respectively. Thus, nucleotide exchange or NTP hydrolysis in the weak site would dramatically change the internal distribution of the intermediates with possible different functions in the helicase functioning, that is, in interactions with the DNA (*68*).

Previous biochemical studies indicated that unwinding of the dsDNA and the ATP hydrolysis can occur at the ATP concentrations where only the strong binding site is engaged in interactions with the cofactor (*22*). However, the nucleotide binding to the weak site seems to increase the efficiency of the unwinding reaction (*22*). The very different energetics, dynamics, structure, and magnesium effect of the weak nucleotide-binding site as compared to the strong site argue for a different role of the weak site in the functioning of the PriA helicase as compared to the strong binding site. Rather, the site that binds fast and releases the nucleotide cofactor with intermediates little affected by magnesium appears to be predominantly an allosteric binding site that functions in controlling the specific interactions with replication fork or PAS sit, and the processivity of the enzyme by, for example, affecting the affinity of the helicase−DNA complex in different states of ligation, achieved through direct nucleotide exchange and/or ATP hydrolysis (*68*).

ACKNOWLEDGMENT

We thank Betty Sordahl for reading the manuscript.

REFERENCES

1. Marians, K. J. (1999) PriA: at the crossroads of DNA replication and recombination, *Prog. Nucleic Acid Res. Mol. Biol. 63*, 39−67.
2. Kornberg, A., and Baker, T. A. (1992) *DNA Replication*, pp 275−293, Freeman, San Francisco.
3. Sangler, S. J., and Marians, K. J. (2000) Role of PriA in replication fork reactivation in *Escherichia coli*, *J. Bacteriol. 182*, 9−13.
4. Lee, M. S., and Marians, K. J. (1987) *Escherichia coli* replication factor Y, a component of the primosome, can act as a DNA helicase, *Proc. Natl. Acad. Sci. U.S.A. 84*, 8345−8349.

5. Lasken, R. S., and Kornberg, A. (1988) The primosomal protein n′ of *Escherichia coli* is a DNA helicase, *J. Biol. Chem. 263*, 5512−5518.
6. Nurse, P., DiGate, R. J., Zavitz, K. H., and Marians, K. J. (1990) Molecular cloning and DNA sequence analysis of *Escherichia coli* priA, the gene encoding the primosomal protein replication factor Y, *Proc. Natl. Acad. Sci. U.S.A. 87*, 4615−4619.
7. Lee, E. H., Masai, H., Allen, G. C., Jr., and Kornberg, A. (1990) The priA gene encoding the primosomal replicative n′ protein of *Escherichia coli*, *Proc. Natl. Acad. Sci. U.S.A. 87*, 4620−4624.
8. Nurse, P., Liu, J., and Marians, K. J. (1999) Two modes of PriA binding to DNA, *J. Biol. Chem. 274*, 25026−25032.
9. Wickner, S., and Hurwitz, J. (1975) Association of phiX174 DNA-dependent ATPase activity with an *Escherichia coli* protein, replication factor Y, required for in vitro synthesis of phiX174 DNA, *Proc. Natl. Acad. Sci. U.S.A. 72*, 3342−3346.
10. Shlomai, J., and Kornberg, A. (1980) A prepriming DNA replication enzyme of *Escherichia coli*. I. Purification of protein n′: a sequence-specific, DNA-dependent ATPase, *J. Biol. Chem. 255*, 6789−6793.
11. Shlomai, J., and Kornberg, A. (1980) A prepriming DNA replication enzyme of *Escherichia coli*. II. Actions of protein n′: a sequence-specific, DNA-dependent ATPase, *J. Biol. Chem. 255*, 6794−6798.
12. McGlynn, P., Al-Deib, A. A., Liu, J., Marians, K. J., and Lloyd, R. G. (1997) The DNA replication protein PriA and the recombination protein RecG bind D-loops, *J. Mol. Biol. 270*, 212−221.
13. Jones, J. M., and Nakai, H. (1999) Duplex opening by primosome protein PriA for replisome assembly on a recombination intermediate, *J. Mol. Biol. 289*, 503−516.
14. Jones, J. M., and Nakai, H. (2001) *Escherichia coli* PriA helicase: fork binding orients the helicase to unwind the lagging strand side of arrested replication forks, *J. Mol. Biol. 312*, 935−947.
15. Lohman, T. M., and Bjornson, K. P. (1996) Mechanisms of helicase-catalyzed DNA unwinding, *Annu. Rev. Biochem. 65*, 169−214.
16. von Hippel, P. H., and Delagoutte, E. (2002) Helicase mechanisms and the coupling of helicases within macromolecular machines. Part I: Structures and properties of isolated helicases, *Q. Rev. Biophys. 35*, 431−78.
17. von Hippel, P. H., and Delagoutte, E. (2003) Helicase mechanisms and the coupling of helicases within macromolecular machines. Part II: integration of helicases into cellular processes, *Q. Rev. Biophys. 36*, 1−69.
18. Matson, S. W., and Kaiser-Rogers, K. A. (1990) DNA helicases, *Annu. Rev. Biochem. 59*, 289−329.
19. Galletto, R., Jezewska, M. J., and Bujalowski, W. (2004) Unzipping mechanism of the double-stranded DNA unwinding by a hexameric helicase. Quantitative analysis of the rate of the dsDNA unwinding, processivity and kinetic step-size of the *Escherichia coli* DnaB helicase using rapid quench-flow method, *J. Mol. Biol. 343*, 83−99.
20. Galletto, R., Jezewska, M. J., and Bujalowski, W. (2004) Unzipping mechanism of the double-stranded DNA unwinding by a hexameric helicase. The effect of the 3′ arm and the stability of the dsDNA on the unwinding activity of the *Escherichia coli* DnaB helicase, *J. Mol. Biol. 343*, 101−114.
21. Zavitz, K. H., and Marians, K. J. (1992) ATPase-deficient mutants of the *Escherichia coli* DNA replication protein PriA are capable of catalyzing the assembly of active primosome, *J. Biol. Chem. 267*, 6933−6940.
22. Lee, M. S., and Marians, K. J. (1990) Differential ATP requirements distinguish the DNA translocation and DNA unwinding activities of the *Escherichia coli* PriA protein, *J. Biol. Chem. 265*, 17078−17083.
23. Moore, J. K., and Lohman, T. M. (1994) Kinetic mechanism of adenine nucleotide binding to and hydrolysis by the *Escherichia coli* Rep monomer. 1. Use of fluorescent nucleotide analogues, *Biochemistry 33*, 14550−14564.
24. Moore, J. K., and Lohman, T. M. (1994) Kinetic mechanism of adenine nucleotide binding to and hydrolysis by the *Escherichia coli* Rep Monomer. 2. Application of a kinetic competition approach, *Biochemistry 33*, 14565−14578.
25. ,Rajendran, S., Jezewska, M. J., and Bujalowski W. (2000) Multiple-step kinetic mechanism of DNA-independent ATP binding and hydrolysis by *Escherichia coli* replicative helicase DnaB protein: quantitative analysis using the rapid quench-flow method, *J. Mol. Biol. 303*, 773−795.
26. Talavera, M. A., and De la Cruz, E. M. (2005) Equilibrium and kinetic analysis of nucleotide binding to the DEAD-box RNA helicase DbpA, *Biochemistry 44*, 959−970.
27. Wong, I., Moore, Bjorson, K. J., Hsieh, J., and Lohman, T. M. (1996) ATPase activity of *Escherichia coli* Rep helicase is dramatically dependent on DNA ligation and protein oligomeric state, *Biochemistry 35*, 57265734.
28. Raney, K. D., Sowers, L. C., Millar, D. P., and Benkovic, S. J. (1994) A fluorescence-based assay for monitoring helicase activity, *Proc. Natl. Acad. Sci. U.S.A. 91*, 6644−6648.
29. Jezewska, M. J., Rajendran, S., and Bujalowski, W. (2000) *Escherichia coli* replicative helicase PriA protein-single-stranded DNA complex. Stoichiometries, free energy of binding, and cooperativities, *J. Biol. Chem. 275*, 27865−27873.
30. Jezewska, M. J., and Bujalowski, W. (2000) Interactions of *Escherichia coli* replicative helicase PriA protein with single-stranded DNA, *Biochemistry 39*, 10454−10467.
31. Galletto, R., Jezewska, M. J., and Bujalowski, W. (2004) Multistep sequential mechanism of *E. coli* helicase PriA protein−ssDNA interactions. Kinetics and energetics of the active ssDNA-searching site of the enzyme. *Biochemistry 43*, 11002−11016.
32. Hiratsuka, T. (1983) New ribose-modified fluorescent analogs of adenine and guanine nucleotides available as substrates for various enzymes, *Biochim. Biophys. Acta 742*, 496−508.
33. Bujalowski, W., and Klonowska, M. M. (1993) Negative cooperativity in the binding of nucleotides to *Escherichia coli* replicative helicase DnaB protein. Interactions with fluorescent nucleotide analogues, *Biochemistry 32*, 5888−5900.
34. Galletto, R., Rajendran, S., and Bujalowski, W. (2000). Interactions of nucleotide cofactors with the *Escherichia coli* replication factor DnaC protein, *Biochemistry 39*, 12959−12969.
35. Bujalowski, W., and Klonowska, M. M. (1994) Structural characteristics of the nucleotide-binding site of *Escherichia coli* primary replicative helicase DnaB protein. Studies with ribose and base-modified fluorescent nucleotide analogues, *Biochemistry 33*, 4682−4694.
36. Bujalowski, W., and Klonowska, M. M. (1994) Close proximity of tryptophan residues and ATP-binding site in *Escherichia coli* primary replicative helicase DnaB protein. Molecular topography of the enzyme, *J. Biol. Chem. 269*, 31359−31371.
37. Jezewska, M. J., Kim, U.-S., and Bujalowski, W. (1996) Interactions of *Escherichia coli* primary replicative helicase DnaB protein with nucleotide cofactors, *Biophys. J. 71*, 2075−2086.
38. Jezewska, M. J., and Bujalowski, W. (1997). Quantitative analysis of ligand-macromolecule interactions using differential quenching of the ligand fluorescence to monitor the binding, *Biophys. Chem. 64*, 253−269.
39. Bujalowski, W., and Jezewska, M. J. (2000) in *Spectrophotometry & Spectrofluorimetry. A Practical Approach* (Gore, M. G., Ed.), pp 141−165, Oxford University Press, Oxford.
40. Bujalowski, W., and Jezewska, M. J. (2000) Kinetic mechanism of nucleotide cofactor binding to *Escherichia* coli replicative helicase DnaB protein. Stopped-flow kinetic studies using fluorescent, ribose-, and base-modified nucleotide analogues, *Biochemistry 39*, 2106−2122.
41. Galletto, R., and Bujalowski, W. (2002) The *E. coli* replication factor DnaC protein exists in two conformations with different nucleotide binding capabilities. 1. Determination of the binding mechanism using ATP and ADP fluorescent analogues. *Biochemistry 41*, 8907−8920.
42. Galletto, R., and Bujalowski, W. (2002) Kinetics of the *E. coli* replication factor DnaC protein−nucleotide interactions. 2. Fluorescence anisotropy and transient, dynamic quenching stopped-flow studies of the reaction intermediates, *Biochemistry 41*, 8921−8934.
43. Bujalowski, W., and Jezewska, M. J. (2000) Kinetic mechanism of the single-stranded DNA recognition by *Escherichia coli* replicative helicase DnaB protein. Application of the matrix projection operator technique to analyze stopped-flow kinetics, *J. Mol. Biol. 295*, 831−852.
44. Jezewska, M. J., Rajendran, S., Galletto, R., and Bujalowski, W. (2001) Kinetic mechanisms of rat polymerase β−ssDNA interactions. Quantitative fluorescence stopped-flow analysis of the formation of the (Pol β)$_{16}$ and (Pol β)$_5$ binding mode, *J. Mol. Biol. 313*, 977−1002.
45. Bujalowski, W., Jezewska, M. J., and Galletto, R. (2002) Dynamics of gapped DNA recognition by human polymerase β, *J. Biol. Chem. 277*, 20316−20327.

46. Rajendran, S., Jezewska, M. J., and Bujalowski, W. (2001) Multiple-step kinetic mechanisms of the ssDNA recognition process by human polymerase β in its different ssDNA binding modes, *Biochemistry 40*, 11794−11810.
47. Lucius, A. L., and Lohman, T. M. (2004) Effects of temperature and ATP on the kinetic mechanism and kinetic step-size for *E. coli* RecBCD helicase-catalyzed DNA unwinding, *J. Mol. Biol. 339*, 751−771.
48. Lohman, T. M., and Bujalowski, W. (1991) Thermodynamic methods for model-independent determination of equilibrium binding isotherms for protein−DNA interactions: spectroscopic approaches to monitor binding, *Methods Enzymol. 208*, 258−290.
49. Jezewska, M. J., and Bujalowski, W. (1996) A general method of analysis of ligand binding to competing macromolecules using the spectroscopic signal originating from a reference macromolecule. Application to *Escherichia coli* replicative helicase DnaB protein−nucleic acid interactions, *Biochemistry 35*, 2117−2128.
50. Hiratsuka, T. (1984) Distinct structures of ATP and GTP complexes in the myosin ATPase, *J. Biochem. 96*, 155−162.
51. Turner, D. C., and Brand, L. (1968) Quantitative estimation of protein binding site polarity. Fluorescence of *N*-arylaminonaphthalenesulfonates, *Biochemistry 10*, 3381−3390.
52. Hill, T. L. (1985) *Cooperativity Theory in Biochemistry. Steady State and Equilibrium Systems*, pp 167−234, Springer-Verlag, New York.
53. Bernasconi, C. J. (1976) *Relaxation Kinetics*, pp 98−129, Academic Press, New York.
54. Hammes, G. G., and Schimmel, P. R. (1970) *The Enzymes. Kinetics and Mechanism*, Vol. II, pp 67−114, Academic Press, New York.
55. Moore, J. W., and Pearson. R. G. (1981) *Kinetics and Mechanism*, Chapter 6, John Wiley & Sons, New York.
56. Berry, R. S., Rice, S. A., and Ross, J. (1980) *Physical Chemistry*, Chapter 15, John Wiley & Sons, New York.
57. Fierke, C. A., and Hammes, G. G. (1995) Transient kinetic approaches to enzyme mechanisms, *Methods Enzymol. 249*, 3−37.
58. Huang, S. G., Weisshart, K., and Fanning, E. (1998) Characterization of the nucleotide binding properties of SV40 T antigen using fluorescent 3′(2′)-*O*-(2,4,6-trinitrophenyl)adenine nucleotide analogues, *Biochemistry 37*, 15336−15344.
59. Kosower, E. M. (1958) The effect of solvent on spectra. I. A new empirical measure of solvent polarity: Z-values, *J. Am. Chem. Soc. 80*, 3253−3260.
60. Abeles, R. H., Frey, P. A., and Jencks, W. P. (1992) *Biochemistry*, pp 791−826, Jones and Bartlett, Boston/London.
61. Walker, J. E., Saraste, M., Runswick, M. J., and Gay, N. J. (1983) Distantly related sequences in the α- and β-subunits of ATP synthase, myosin, kinases, and other ATP-requiring enzymes and a common nucleotide binding fold, *EMBO J. 1*, 945−951.
62. Saraste, M., Sibbald, P. R., and Wittinghofer, A. (1990) The P-loop−a common motif in ATP- and GTP-binding proteins, *Trends Biochem. Sci. 5*, 430−432.
63. Myles. G. M., Hearst, J. E., and Sancar, A. (1991) Site-specific mutagenesis of conserved residues within Walker A and B sequences of *Escherichia coli* UvrA protein, *Biochemistry 30*, 3824−3834.
64. Korolev, S., Hsieh J., Gauss G. H., Lohman T. M., and Waksman G. (1997) Major domain swiveling revealed by the crystal structures of complexes of *E. coli* Rep helicase bound to single-stranded DNA and ADP, *Cell 90*, 635−647.
65. Myles. G. M., Hearst, J. E., and Sancar, A. (1991) Site-specific mutagenesis of conserved residues within Walker A and B sequences of *Escherichia coli* UvrA protein, *Biochemistry 30*, 3824−3834.
66. Gorbalenya, A. E., and Koonin, E. V. (1993) Helicases: amino acid sequence comparisons and structure−function relationships, *Curr. Opin. Struct. Biol. 3*, 419−429.
67. Lucius, A. L., Jezewska, M. J., and Bujalowski, W. (2006) The *Escherichia coli* PriA helicase has two nucleotide-binding sites differing dramatically in their affinities for nucleotide cofactors. 1. Intrinsic affinities, cooperativities, and base specificity of nucleotide cofactor binding, *Biochemistry 45*, 7202−7216.
68. Lucius, A. L., Jezewska, M. J., and Bujalowski, W. (2006) Allosteric interactions between the nucleotide-binding sites and the ssDNA-binding site in the PriA helicase−ssDNA complex. 3, *Biochemistry 45*, 7237−7255.

BI051827E